# The Ser/Thr kinase PrkC participates in cell wall homeostasis and antimicrobial resistance in Clostridium difficile

Elodie Cuenot, Transito Garcia-Garcia, Thibaut Douche, Olivier Gorgette, Pascal Courtin, Sandrine Denis-Quanquin, Sandra Hoys, Yannick D.N. Tremblay, Mariette Matondo, Marie-Pierre Chapot-Chartier, et al.

# The Ser/Thr kinase PrkC participates in cell wall homeostasis and antimicrobial resistance in *Clostridium difficile*

Elodie Cuenot[1,2], Transito Garcia-Garcia[1,2], Thibaut Douche[3], Olivier Gorgette[4], Pascal Courtin[5], Sandrine Denis-Quanquin[6], Sandra Hoys[7], Yannick D.N. Tremblay[1,2], Mariette Matondo[3], Marie-Pierre Chapot-Chartier[5], Claire Janoir[7], Bruno Dupuy[1,2], Thomas Candela[7] and Isabelle Martin-Verstraete[1,2*]

[1] Laboratoire Pathogénese des Bactéries Anaérobies, Institut Pasteur, Paris, France
[2] Université Paris Diderot, Sorbonne Paris Cité, Paris, France
[3] Plateforme Protéomique, Unité de Technologie et service Spectrométrie de masse pour la biologie, CNRS USR 2000, Institut Pasteur, Paris, France
[4] Unité Technologie et service Biolmagerie Ultrastructurale, Institut Pasteur, Paris, France
[5] Micalis Institute, INRA, AgroParisTech, Université Paris-Saclay, Jouy-en-Josas, France.
[6] Univ Lyon, Ens de Lyon, CNRS, Université Lyon 1, Laboratoire de Chimie UMR 5182, F-69342, Lyon, France
[7] EA 4043, Unité Bactéries Pathogènes et santé (UBaPS), Univ. Paris-Sud, Université Paris-Saclay, 92290 Châtenay-Malabry, France

*Corresponding author

running title: The PASTA Ser/Thr kinase of *Clostridium difficile*

Keywords: Hanks kinase, cephalosporin sensitivity, cell morphology, envelope homeostasis, CAMPs, biofilms, peptidoglycan

Abstract:

*Clostridium difficile* is the leading cause of antibiotic-associated diarrhea in adults. During infection, *C. difficile* must detect the host environment and induce an appropriate survival strategy. Signal transduction networks involving serine/threonine kinases (STKs) play key roles in adaptation, as they regulate numerous physiological processes. PrkC of *C. difficile* is a STK with two PASTA domains. We showed that PrkC is membrane associated and is found at the septum. We observed that deletion of *prkC* affects cell morphology with an increase in mean size, cell length heterogeneity, and presence of abnormal septa. When compared with the wild-type strain, a Δ*prkC* mutant was able to sporulate and germinate but was less motile and formed more biofilm. Moreover, a Δ*prkC* mutant was more sensitive to antimicrobial compounds that target the cell envelope such as the secondary bile salt deoxycholate, cephalosporins, cationic antimicrobial peptides, and lysozyme. This increased susceptibility was not associated with differences in peptidoglycan or polysaccharide II composition. However, the Δ*prkC* mutant had less peptidoglycan and released more polysaccharide II into the supernatant. A proteomic analysis showed that the majority of *C. difficile* proteins associated with the cell wall were less abundant in the Δ*prkC* mutant compared to the wild-type strain. Finally, in a hamster model of infection the Δ*prkC* mutant had a colonization delay that did not significantly affect overall virulence.

## Introduction

*Clostridium difficile* is the leading cause of antibiotic-associated infections in adults. Severity of *C. difficile* infection (CDI) symptoms range from diarrhea to life-threatening pseudo-membranous colitis. Major risks associated with CDI include antibiotic exposure leading to dysbiosis of gut microbiota, as well as, advanced aged and hospitalization (1). The impact of CDI is significant in terms of mortality, morbidity, disease management and financial burden. With the emergence of new isolates, the incidence and severity of CDI have increased both in North America and Europe (2). *C. difficile* is acquired from the environment through the ingestion of spores. This resistant form of the bacterium is thought to be responsible for transmission, environmental persistence and dissemination. When the normal intestinal microbiota is disrupted, the pools of metabolites present in the gut change leading to an increased concentration of cholate conjugates, which in turn triggers spore germination (3, 4). The vegetative cells can then multiply and colonize the dysbiotic gastrointestinal tract. Toxigenic strains of *C. difficile* produce two toxins, TcdA and TcdB, which are its main virulence factors. These toxins cause alteration of the actin cytoskeleton of epithelial cells and neutrophil recruitment causing local inflammation (3). Following the administration of a targeted antibiotic therapy such as metronidazole or vancomycin, CDI relapse can occur, involving spore and possibly biofilm formation (5, 6). Additional factors including those involved in stress adaptation and surface associated proteins, such as adhesins, the fibronectin-binding protein (FbpA), the surface layer protein (SlpA) and the flagellum also participate in the colonization process, allowing *C. difficile* to establish its intestinal niche (7).

Gut dysbiosis is an essential step that allows *C. difficile* to colonize the colon and cause an infection. Certain antibiotics such as cephalosporins, clindamycin and fluoroquinolones are known to increase the risk of developing a CDI. Most of *C. difficile* strains are resistant to these antibiotics, which is of major concern (1). Fluoroquinolone resistance in *C. difficile* strains is associated with amino acid substitution in the gyrases GyrA or GyrB (1). The mechanisms responsible for cephalosporin resistance by *C. difficile* remain poorly characterized (1). However, some progress has been made, as a class D ß-lactamase was identified in the genomes of most *C. difficile* strains (8). In addition to antibiotics, vegetative cells also encounter secondary bile salts (4), host secreted antimicrobial peptides and also reactive oxygen and nitrogen species produced during inflammation (3, 9). To survive in the host, *C. difficile* must detect the host environment and induce an appropriate survival strategy, which may include activating the general stress response, sporulation, biofilm formation, and pro-

ducing virulence factors (5, 6, 9).

Protein phosphorylation is a reversible post-translational modification used to transduce signal and regulate cellular processes. Bacterial serine/threonine kinases of the Hanks family (STKs) share structural similarities with eukaryotic serine/threonine kinases and undergo substrate phosphorylation on serine or threonine residues (10). STKs and their associated phosphatases (STP) regulate numerous physiological processes including translation, carbon and cell-wall metabolism, antibiotic tolerance, cell division, developmental processes, and virulence (10, 11). Phosphoproteomic studies revealed that STKs might phosphorylate a broad spectrum of substrates (12) including enzymes, components of the cellular machinery involved in translation, division or repair and also several transcriptional regulators that mainly form part of two-component systems (10, 13). Therefore, STKs are key integration nodes in signaling networks that control bacterial physiology, growth and stationary phase. In *B. subtilis*, PrkC is a trans-membrane kinase with an extracellular signal receptor domain containing penicillin-binding and STK associated (PASTA) repeats. PrkC interacts with peptidoglycan fragments and ß-lactam *in vitro* (14, 15), while a PASTA-STK (Stk1) homologue in *Staphylococcus aureus* interacts with lipid II (16). In *B. subtilis*, PrkC is a key-signaling enzyme that controls stationary phase survival, biofilm formation, sporulation, germination (13) and peptidoglycan (PG) metabolism (17). Inactivation of genes encoding PASTA domain-containing STKs are associated with a range of phenotypes among Gram-positive bacteria, with defects in cell division and changes in cell-wall metabolism commonly observed (10, 17, 18). In *S. aureus*, Stk1 plays a role in virulence, antibiotic resistance and cell-wall remodeling (17) whereas in *Streptococcus pneumonia*, StkP controls cell division, competence, virulence, adherence to eukaryotic cells, stress response and cell wall metabolism (17, 19).

The role of STKs has not been studied in anaerobic firmicutes. *C. difficile* has two genes encoding STKs, *CD2148* and *prkC* (*CD2578*) and one gene encoding a STP (*CD2579*). In this study, we characterized the role of the *C. difficile* PASTA-STK, PrkC, in the regulation of the physiological processes important in CDI. Inactivation of the *prkC* gene resulted in changes in the morphology and the properties of the cell envelope as well as increased sensitivity to antimicrobial compounds targeting the cell wall.

## Materials and methods

### Bacterial strains and growth conditions

*C. difficile* strains and plasmids used in this study are listed in Table S1. *C. difficile* strains were grown anaerobically (5% $H_2$, 5% $CO_2$, 90% $N_2$) in TY broth (Bacto tryptone 30 $g.l^{-1}$, yeast extract 20 $g.l^{-1}$, pH 7.4), in Brain Heart Infusion broth (BHI) or in a peptone-containing medium (Pep-M) (20). Sporulation medium (SM) (21) was used for sporulation assays and spores were produced in SMC medium (22). Solid media were obtained by adding agar to a final concentration of 17 $g.l^{-1}$. When necessary, cefoxitin (Cfx, 25 $\mu g.ml^{-1}$) or thiamphenicol (Tm, 15 $\mu g.ml^{-1}$) was added. *E. coli* strains were grown in LB broth. When indicated, ampicillin (100 $\mu g.ml^{-1}$) or chloramphenicol (15 $\mu g.ml^{-1}$) was added. Anhydrotetracycline (ATc) was used to induce expression of the *prkC* gene from the $P_{tet}$ promoter of pDIA6103 (23).

**Construction of plasmids and strains**

The allelic exchange cassette used to delete of the *CD2578* gene *(prkC)* was constructed in a derivative of pMTLSC7315 (24) lacking the multi-cloning site. DNA sequences flanking the *prkC* gene (1038 and 1117-bp) were amplified by PCR using primers IMV854 and IMV855 or IMV856 and IMV857 (Table S2 and Fig S1). A DNA fragment obtained by overlapping PCR was digested by XhoI and BamHI and then ligated into pMTLSC7315ΔMCS, giving pDIA6401. *E. coli* HB101 (RP4) containing pDIA6401 was mated with *C. difficile* 630Δ*erm*. Transconjugants were selected on BHI-Cfx-Tm plates. Colonies were restreaked onto the same medium to identify faster growing single-crossover integrants that were then streaked onto CDMM supplemented with 50 μg/ml fluorocytosine (FC) to select for second cross-over events. $FC^R$ $Tm^S$ clones that have lost pDIA6401 were analyzed by PCR using IMV867 and IMV868 to distinguish between wild-type and Δ*prkC* clones (Fig S1). For complementation, the *prkC* gene (positions -22 to +2205 from the translational start site) was amplified using primers IMV879 and IMV880. The PCR fragment was cloned between the StuI and BamHI sites of pDIA6103 (25) to produce pDIA6413. To construct a plasmid expressing PrkC-HA (pDIA6713), an reverse PCR was performed using pDIA6413 as template and primers EC01 and EC02. The same strategy was used to introduce a point mutation into the *prkC* gene [lysine at position 39 replaced by an alanine (K39→A)]. The resulting plasmid, pDIA6714, was then used to construct pDIA6716 expressing HA-tagged *prkC*(K39→A). These plasmids were transferred into *C. difficile* strains by conjugation (Table S1).

To construct a translational SNAP-PrkC fusion, we amplified the SNAP coding sequence fused to a linker in 3' (GGATCCGCAGCTGCT) using pFT58 as a template and primers EC238 and EC239. pDIA6413 (pDIA6103-*prkC*) was amplified by inverse PCR using the

primers EC236 and EC237. Using these two fragments, pDIA6855 was obtained by Gibson Assembly. pDIA6855 was conjugated in the 630Δ*erm* strain to obtain CDIP1357 (Table S1). To determine if *prkC* is co-transcribed with upstream genes (*CD2579* and *rlmN*), we carried out an RT-PCR experiment using RNA extracted from exponentially growing cells. After cDNA synthesis using IMV843, a primer targeting the *prkC* gene, PCR amplification was tested with pairs of primers located in adjacent genes (*prkC*/*CD2579* or *CD2579/rlmN*). Non-treated RNAs were used as a negative control.

**Antimicrobial sensitivity tests**

Cultures of *C. difficile* strains ($OD_{600nm}$ of 0.3) were plated on BHI agar plates. 6-mm paper disks containing antibiotics were placed onto the agar surface. Lysozyme (800 µg) was also placed on a 6-mm paper disk using Pep-M agar plates. The growth inhibition diameter was measured after 24 h of incubation at 37°C. Minimal Inhibitory Concentrations (MICs) were determined on BHI plates by E-test (bioMérieux) after 24 h incubation at 37°C. To test susceptibility for antimicrobial peptides, protocols were modified from previous published work (26, 27). Each well of a 24-well microplate was inoculated with 1 ml of a BHI bacterial inoculum ($OD_{600nm}$ of 0.01). After addition of bacitracin (Sigma Aldrich), polymixin B (Sigma Aldrich) or nisin (Sigma Aldrich), microplates were incubated at 37°C for 20 h. The MIC was defined as the lowest concentration of antimicrobial peptide preventing growth.

5 µl of an overnight culture of *C. difficile* strains was streaked on BHI plates without or with SDS (0.005% to 0.009%). The plates were incubated at 37°C for 48 h. Deoxycholate (DOC) resistance tests were performed in 24-well microplates. Each well was inoculated with 1 ml of TY with or without DOC (0.03%). The $OD_{600nm}$ of each culture was monitored. For autolysis, cells ($OD_{600nm}$ of 1) were resuspended in 50 mM potassium phosphate buffer (pH 7.0) containing 0.01 % of Triton X-100 and incubated at 37°C. The $OD_{600nm}$ was determined every 5 min.

**Sporulation, germination, motility and biofilm formation assays**

Sporulation assays were performed as described previously (28). To purify spores, 100 µl of culture plated on solid SMC were grown at 37°C for 7 days. Spores were scraped off with water and then incubated 7 days at 4°C to allow the release of spores from the cells. Spores were purified by centrifugation using a HistoDenz (Sigma-Aldrich) gradient as described previously (22). For the germination efficiency tests, we monitored $OD_{600nm}$ of purified spores incubated under anaerobiosis in BHIS supplemented with 0.5 % taurocholate, with bryostatin or muropeptides.

To measure motility, plates containing 25 ml of BHI agar (0.3% w/v), Tm and ATc were inoculated with 5 µl of an exponential-phase culture. Plates were incubated for 48h at room temperature and the zone of motility was then measured. For the biofilm assay, 1 ml of BHI-S medium containing 0.1 M glucose, 0.1% cysteine and polymixin B (20 $\mu g.ml^{-1}$) or DOC (0.01%) was inoculated and deposited in a well of a 24-well microplate. Microplates were incubated at 37°C. The biofilm was washed with PBS (Phosphate buffered saline), stained with 1 ml of crystal violet (0.2%) followed by two washes with PBS. The $OD_{570nm}$ was measured after resuspension of the cells in methanol/acetone (80%/20%) using non-inoculated medium as a negative control. For dispersion of preformed biofilms, 24 h and 48 h biofilms were treated with DNase I (100 µg/ml in 150 mM NaCl, 1 mM $CaCl_2$) under an-aerobic conditions at 37°C for 1 h (29). Control wells were treated with buffer without DNase. Biofilms were then washed, stained, and quantified as described above.

**Phase contrast and transmission electron microscopy**

*C. difficile* strains were grown 5 h in TY medium. For phase contrast microscopy, cells were analyzed using an axioskop microscope (Zeiss). For transmission electron microscopy (TEM), cultures were mixed with 1 volume of a fixative solution containing 4% paraformal-dehyde (PFA) and 4% glutaraldehyde (GA) in PHEM buffer 1x pH 7.3 (60 mM Pipes, 25mM Hepes, 10 mM EGTA, 2mM $MgCl_2$) and then incubated for 30 min at room tempera-ture. After centrifugation, pellets were resuspended in a second fixative solution (2% PFA and 2% GA in PHEM buffer pH= 7.3) and incubated for 1 h. Samples were then washed twice in PBS prior to being subjected to a high pressure (>2000 bar) freezing in 1-hexadecane using a BAL-TEC HPM 010 (LEICA). Freeze substitution was done with 2% $OsO_4$ in acetone followed by several steps: -90°C for 42 h, warmed up to −30°C (5°C/h), incubated for 12 h, warmed up to 0°C (10°C/h) and incubated for 1h. Samples were then washed with acetone on ice and incubated in EPON/acetone at different volume ratio (1/3 for 3 h, 1/1 for 3 h; 2/1 ON; 3/1 for 4 h), followed by an incubation in pure EPON (2 h, overnight; 6 h). Samples were then incubated overnight in EPON and the hardener BDMI prior to polymerization at 60°C for 48 h. Sections (60-70 nM) were obtained on a FC6/UC6 ultramicrotome (Leica), transferred on 200 Mesh Square Copper grids coated with formvar and carbon (CF-200-Cu50, Delta Microscopy). Samples were stained with 4% uranyl acetate and counterstained with lead citrate. Images were recorded with TECNAI SPIRIT 120 kv (with a bottom-mounted EAGLE 4Kx4K Camera).

**SNAP labelling, fluorescence microscopy and image analysis**

For membrane and chromosome staining, 500 µl of exponential-phase cells were centrifuged and resuspended in 100 µl of PBS containing the fluorescent membrane dye FM 4-64 (1 µg/ml, Molecular Probes, Invitrogen) and the DNA stain 4,6-Diamidino-2-phenylindole (DAPI) (2 µg/ml, Sigma). Samples were incubated for 2 min in the dark and mounted on 1.2% agarose pad. Strain CDIP1357 was grown 2 h in TY and expression of the $SNAP^{Cd}$-*prkC* fusion was induced with 50 ng/ml of ATc for 2 h. For SNAP labelling, the TMR-Star substrate (New England Biolabs) was added at 250 nM, and the mixture was incubated for 30 min in the dark under anaerobiosis. Cells were then collected by centrifugation, washed and resuspended in PBS. Cell suspension (3 µl) was mounted on 1.7% agarose-coated glass slides. The images were taken with 300 ms exposure times for the autofluorescence and 900 ms exposure times for the SNAP using a Nikon Eclipse TI-E microscope 100x Objective and captured with a CoolSNAP HQ2 Camera. The images were analysed using ImageJ (30).

**Detection of phospho-threonine by western blot on soluble and insoluble fractions.**

Cells were grown for 6 h in TY and then harvested by centrifugation. The pellets were re-suspended in PBS containing protease and phosphatase inhibitor cocktails (Sigma-Aldrich) and 0.12 µg/ml of DNase. Cells were lysed for 45 min at 37°C and then centrifuged. The soluble fraction was diluted twice with 2X Sample buffer (150 mM Tris-HCl pH6.8, 30% glycerol, 1.5 % SDS, 15% β-mercaptoethanol, 2 µg/ml of bromophenol blue). After 2 washes with PBS, the insoluble fraction was resuspended in 2X PBS containing 1% SDS, and mixed with 2X Sample buffer. Western blots were performed using an anti-P-Thr primary antibody (Cell signaling) followed by a goat anti-rabbit horseradish-peroxidase-conjugated secondary antibody (Sigma-Aldrich) and developed using the SuperSignalWest Femto chemiluminescent Kit (Thermo scientific).

**Peptidoglycan and polysaccharide II analysis**

Peptidoglycan (PG) samples were prepared from 1.5 l of *C. difficile* grown in BHI ($OD_{600nm}$ of 1) as previously described (31). Purified PG was then digested with mutanolysin (Sigma Aldrich) and the soluble muropeptides were separated by reverse phase high-performance liquid chromatography (RP-HPLC) (31). Polysaccharides II (PSII) were extracted from *C. difficile* grown in BHI ($OD_{600nm}$ of 1) as previously described (32). PSII was lyophilized and its structure was checked by [$^{1}$H] and [$^{13}$C] NMR. Spectra were acquired on a 400 MHz Bruker spectrometer equipped with a Prodigy probe. PSII was lyophilized and its structure was determined by [$^{1}$H] NMR. For the quantification of PG and PSII, 500 ml of culture ($OD_{600nm}$ of 1) was used to purify PSII covalently linked to PG (PG-PSII). PG-PSII was purified as previously described (33) without the acetone treatment. Linkage between PG and

PSII was disrupted after an incubation for 48 h at 4°C in hydrofluoric acid (48%). The pellet containing PG was washed three times in $H_2O$ and the hydrofluoric acid supernatant that contains PSII subunits was evaporated and resuspended in $H_2O$. Both, PG and PSII were lyophilized and then weighted.

For the PSII dot blot, exponential phase cultures were harvested by centrifugation. Supernatant and total crude cell extracts were kept as separate fractions. The supernatant fraction was recovered and precipitated with 10% TCA for 30 min. The supernatant and the total crude cell fractions were treated with 100 µg/ml of proteinase K (Sigma) for 1 h at 37°C. Samples were then serially diluted and 5 µl of each dilution were spotted onto an activated polyvinylidene difluoride membrane. The membrane was washed in $H_2O$, blocked for 15 min in TBST (20 mM Tris-HCl, 150 mM NaCl, 0.05% Tween20, pH7.5) containing 10% milk, and then washed in 5% milk in TBST for 2 min. After overnight incubation in PSII-LTB rabbit antiserum (1:8,000) (34), the membrane was washed once in TBST with 5% milk, twice in TBST for 5 min, and once in TBST with 5% milk for 10 min. Following incubation with goat anti-rabbit horseradish-peroxidase-conjugated secondary antibody at 1:10,000 dilution for 1 h, the membrane was washed 5 times in TBST for 5 min, and revealed using the SuperSignalWest Femto chemiluminescent substrate.

**Isolation of cell-wall proteins and proteomic analysis**

*C. difficile* strains were grown for 6 h in TY at 37°C and 20 mL of each culture was then centrifuged. The cell pellets were washed with PBS, resuspended ($OD_{600nm}$ of 100) in 75 mM Tris-HCl pH6.8, 15% glycerol, 7.5% β-mercaptoethanol, 0.75% SDS and boiled for 10 min at 100°C. Proteins were precipitated with 10% TCA, washed with 90% cold acetone, dried, resuspended in urea 8 M/$NH_4HCO_3$ 100 mM and sonicated. Total protein extracts (50 µg) were reduced with TCEP (10 mM) (Sigma) for 30 min and alkylated with iodoacetamide 20 mM (Sigma) for 1 h. Proteins were digested with rLys-C 1 µg (Promega) for 4 h at 37°C and with Trypsin 1µg (Promega) overnight at 37°C. The digestion was stopped with Formic acid (FA) 4%. Peptides were desalted on C18 Sep-Pak Cartridge (WAT054955, Waters) and eluted with Acetonitrile (ACN) 50%/FA 0.1% and then ACN 80%/FA 0.1% before being dried in vacuum centrifuge. Peptides were resuspended with ACN 2%/FA 0.1%. A nanochromatographic system (Proxeon EASY-nLC 1000, Thermo Fisher Scientific) was coupled on-line to a Q Exactive™ HF Mass Spectrometer (Thermo Fisher Scientific). Peptides (1 µg) were injected onto a 47 cm C18 column (1.9 µm particles, 100 Å pore size, ReproSil-Pur Basic C18, Dr. Maisch GmbH) and separated with a gradient from 2 to 45 % ACN at a flow rate of 250 nl/min over 132 min. Column temperature was set to 60°C. Data were ac-

quired as previously described (35). Raw data were analyzed using MaxQuant software version 1.5.1.2 (36) using the Andromeda search engine (37). The MS/MS spectra were searched as previously described (35) against an internal *C. difficile* database containing 3,957 proteins and the contaminant file included in MaxQuant. The statistical analysis was performed with Perseus 1.5.2.6 (38) as previously described (35). Missing values for LFQ intensities were imputed and replaced by random LFQ intensities that are drawn from a normal distribution at the low detection level. Statistical significance was assessed with a two-sided *t*-test of the Log2 transformed LFQ intensities with a permutation-based FDR calculation at 5% and S0=2 (39). Differentially regulated proteins are visualized on a Volcano-Plot. The mass spectrometry proteomics data have been deposited to the ProteomeXchange Consortium via the PRIDE (40) partner repository with the dataset identifier PXDX012241.

**Golden Syrian hamster infections**

Golden Syrian hamsters were first treated with a single oral dose of 50 mg/kg of clindamycin. Five days after the antibiotics treatment, the hamsters were infected by gavage with 5000 spores of either the 630Δerm strain or the Δ*prkC* mutant. Spore inocula were standardized before challenge. Eight animals per strain per experiment were used for the infection and we performed two independent experiments. Colonization was followed by enumeration of *C. difficile* cells in feces samples and was started 2-day post infection and each day until the death of the animal. Briefly, feces were resuspended in PBS at 10 $mg.ml^{-1}$ and serially diluted with PBS before plating on BHI supplemented with 3% of defibrinated horse blood and the *C. difficile* selective supplement containing cycloserine (25 µg/ml) plus cefoxitine (8 µg/ml). All animal experiments were conducted according to the European Union guidelines for the handling of laboratory animals and Procedures for infection, euthanasia, and specimen collection were approved by the Central Animal Care Facilities and Use committee of University Paris-Sud (agreement 92-019-01; protocol number 2012-107).

## Results

**CD2578 is the PASTA-STK of *C. difficile***

CD2578 (PrkC) from *C. difficile* contains a cytosolic N-terminal kinase domain and an extracellular motif containing repeats of a PASTA that are separated by a trans-membrane segment (Fig 1A). Based on its predicted amino acid sequence, the kinase domain of PrkC has a high level of sequence identity with that of *B. subtilis* (PrkC), *S. aureus* (Stk1), *S. pneumoniae* (StkP), *Enteroccoccus faecalis* (IreK) and *Mycobacterium tuberculosis* (PknB) (43 to 50%). The conserved lysine within the ATP-binding P loop of the kinase domain is

present and corresponds to position 39 in PrkC (Fig 1A). This residue is essential for the phosphotransfer in other STKs (41). As observed for the PASTA-STKs in other firmicutes, a trans-membrane segment is predicted from amino acid 375 to 397 (42, 43). The extracellular sequence of PrkC contains 2 PASTA motifs (Fig 1A) while up to 7 PASTA motifs are typically present in STKs of other firmicutes (17). Interestingly, *C. difficile* contains a very atypical Ser-Gly-Asn (SGN) rich region of 100 amino acids at the C-terminal part of the protein (Fig 1A). This SGN-rich region is absent from PASTA-STKs of other firmicutes. Interestingly, SGN-rich regions are found in some cell wall anchored proteins of bacilli and in CwpV, a surface associated protein in *C. difficile* but their function have yet to be characterized.

**The *prkC* locus of *C. difficile***

The *prkC* gene likely belongs to a large cluster of genes, which ranges from *dapF* (*CD2590)* to *CD2578-prkC* (Fig 2A). As usually observed in other firmicutes (44, 45), a gene (*CD2579-stp*) encoding a PP2C-type phosphatase (STP), which is probably involved in the dephosphorylation of the PrkC substrates, is adjacent to *prkC*. Upstream of *stp*, we found genes encoding proteins involved in translation (*rlmN*, *rsmB*, *def* and *fmt*), transcription (*rpoZ*), DNA replication (*priA*) and metabolism (*gmk* and *coaBC*). This cluster is conserved in *B. subtilis* and *B. cereus* with the exception of 3 genes that are only present in *C. difficile*; *CD2582* and *CD2583* encoding membrane proteins and *dapF* encoding a diaminopimalate epimerase (Fig 2A). To determine if *prkC* is co-transcribed with *stp* as observed in other firmicutes, and the other genes located upstream of *stp* such as the *rlmN* gene, RT-PCR experiments were performed. PCR products were detected using primer pairs located in adjacent genes (*prkC*/*stp* or *stp/rlmN*) with RNAs processed by a reverse transcriptase but not with untreated RNA used as negative control (Fig 2B). This result indicated that the *prkC* gene is in operon with *stp* but also *rlmN*. Using a genome-wide transcriptional start site (TSS) mapping (25), we identified a unique TSS in the *prkC* locus located 23 bp upstream of *dapF* suggesting that this gene might be the first gene of a large operon. We found a TG-N-TATAAT extended -10 box specific for the consensus of $\sigma^A$-dependent promoters upstream of the TSS (Fig 2A). However, we cannot exclude the existence of additional promoters between *dapF* and *prkC* that were not identified in the genome-wide TSS mapping (25).

**Localization of the PrkC protein**

To determine the cellular location of PrkC, we expressed the *prkC* gene fused to a HA tag under the control of the inducible promoter $P_{tet}$ (pDIA6103-$P_{tet}$-*prkC*-HA*)*. A western blot analysis of the membrane or cytoplasmic fraction with an anti-HA antibody revealed two bands corresponding to proteins of about 100 kDa and 50 kDa (Fig S2A). These two proteins were only detected in the membrane fraction (Fig 1B). The expected molecular weight of the PrkC-HA tagged protein is around 75 kDa and the band detected around 100 kDa likely corresponds to PrkC-HA. Indeed, the PrkC and StkP proteins of *B. subtilis* and *S. pneumoniae* are detected with an apparent molecular weight higher than their expected size (42, 43) and the phosphorylation of the kinase results in a reduced electrophoretic mobility (46). The lower band at 50 kDa could be a form of degradation product that might correspond to the extracellular domain fused to HA. It is worth noting that PrkC of *B. subtilis* is sensitive to protease cleavage (42).

To determine the localization of PrkC, we used a 630Δ*erm* strain containing a plasmid encoding a $SNAP^{Cd}$-PrkC protein fusion produced under the control of the $P_{tet}$ promoter. The production of the $SNAP^{Cd}$-PrkC protein is stable as shown by western blot using an anti-SNAP antibody (Fig S2B). After 2 h of induction, we detected the $SNAP^{Cd}$-PrkC fusion protein fusion at the septum of dividing cells (Fig 1C). Thus, the PrkC protein is membrane associated and localizes at the septum during cell growth.

**Deletion of the *prkC* gene in *C. difficile* and detection of PrkC activity**

To study the role of PrkC in the physiology of *C. difficile*, we inactivated the *prkC* gene by allelic exchange in the strain 630Δ*erm* (24). Deletion of the *prkC* gene from codon two to the stop codon was confirmed by PCR (Fig S1). The *prkC* mutant was complemented with the wild-type *prkC* gene (pDIA6103-$P_{tet}$-*prkC*) or a modified copy of *prkC* (pDIA6103-$P_{tet}$-*prkC*-K39→A) with the lysine residue required for phosphotransfer replaced by an alanine.

The kinase activity of PrkC was demonstrated by comparing the profiles of phosphorylation of the wild-type (WT) strain or the Δ*prkC* mutant carrying either pDIA6103, pDIA6103-$P_{tet}$-*prkC* or pDIA6103-$P_{tet}$-*prkC*-K39→A. We assumed that PrkC and PrkC-K39→A were produced to the same level and were located in membrane because we detected similar levels in the membrane fraction of these proteins with an HA tag fusion (PrkC-HA or PrkC-K39→A-HA) (Fig S2A). We detected proteins phosphorylated on threonine in the WT strain both in soluble and insoluble fractions by western blot analysis with an antibody against phosphorylated threonine residues (α-PThr (Fig 1D). Some bands that were detected in the WT strain and with a lower intensity in the complemented strain disappeared in the Δ*prkC* mutant and

386 in the strain producing a modified PrkC-K39→A protein. This result strongly suggested that
387 PrkC has a kinase activity *in vivo* and that the lysine at position 39 (Fig 1A) is essential for
388 the phosphorylation of PrkC targets as observed in the PASTA-STKs of other firmicutes (17,
389 41).
390
391 **Impact of *prkC* deletion on growth, sporulation and germination**
392 The 630Δ*erm* strain and the Δ*prkC* mutant exhibited nearly identical doubling time and
393 growth yield in TY (Fig S3A). No difference in CFU was also observed between the two
394 strains (Fig S4A and data not shown). We also performed co-culture of the WT and Δ*prkC*
395 mutant strains in TY (Fig S3C). We observed that the Δ*prkC* mutant was less abundant than
396 the wild-type strain by two-fold after 8 h or 24 h of growth. This suggests that there is no
397 drastic difference in fitness associated with the inactivation of *prkC*. The growth of the
398 Δ*prkC* containing pDIA6103-$P_{tet}$-*prkC* was similar to that of the WT strain in the presence of
399 15 ng/ml of ATc but was affected when we added 50 ng/ml of ATc (Fig S3B). This growth
400 defect was also observed in the Δ*prkC* mutant expressing *prkC*-K39→A (Fig S3B). In con-
401 trast, the addition of increasing concentrations of ATc had no effect on the growth of the WT
402 strain harboring an empty plasmid (Fig S3B). A qRT-PCR analysis also showed that expres-
403 sion of *prkC* was similar in the WT and complemented strains in the presence of 15 ng/ml of
404 ATc (Fig S3D). In the presence of 50 ng/ml of ATc, the expression of *prkC* probably in-
405 creased in the Δ*prkC* strain containing pDIA6103-$P_{tet}$-*prkC* because we detected a drastic
406 overproduction of the SNAP-PrkC fusion in the presence of 50 ng/ml when compared to 20
407 ng/ml (Fig S2). Over-production of PrkC is likely responsible for the growth defect observed
408 in the presence of 50 ng/ml of ATc suggesting that a proper level of *prkC* expression is im-
409 portant for the fitness of *C. difficile*. Since the kinase activity of PrkC is apparently not re-
410 sponsible for the growth defect when the protein is overexpressed, the trans-membrane seg-
411 ment or the extracellular domain are probably involved in this toxicity.
412 To determine if PrkC is involved in sporulation, we measure sporulation levels of the WT
413 and the Δ*prkC* mutant strains after 24 h or 72 h of growth in SM. No significant differences
414 were observed between both strains for the quantity of spores produced (Fig S4A). When we
415 tested the ability of purified spores to germinate, we observed that the drop in the $OD_{600nm}$ of
416 spore suspensions after the addition of taurocholate was similar for the WT and the Δ*prkC*
417 mutant (Fig S4 B). In *B. subtilis*, PrkC is involved in the germination of spores in the pres-
418 ence of *B. subtilis* muropeptides (47). However, purified muropeptides from *C. difficile* (0.1
419 to 0.01 mg/ml) failed to induce spore germination of the WT or the Δ*prkC* mutant (data not

shown). Bryostatin is a molecule involved in STK activation that induces germination of *B. subtilis* spores (47). This compound at 1 µM or 10 µM had no effect on *C. difficile* spores (data not shown). All these results indicated that PrkC is not involved in the control of sporulation and spore germination in *C. difficile*.

### *prkC* deletion affects cell morphology

To determine if deletion of *prkC* had an effect on the cell morphology, we analyzed by phase contrast microscopy cells of the 630Δ*erm* strain, the Δ*prkC* mutant, and the complemented strain during exponential growth phase (Fig S5A). The Δ*prkC* mutant cells were more elongated than those of the WT strain and the complemented strain (Fig S5A). We then measured the cell size using cells labeled with DAPI and FM4-64 (Fig 3A and 3B). The Δ*prkC* mutant cells had an average cell size of 9.2 µm whereas the WT and the complemented strains had an average cell size of 4.5 µm and 6.4 µm, respectively (Fig 3B). We detected elongated cells (Fig 3A, blue arrows) and cells with several septa and undivided (Fig 3A, green arrows). Interestingly, we observed septation defects for the Δ*prkC* mutant (Fig 3A, white square, Fig 3C and Fig S5B). Our analysis revealed that 4% of the cells had abnormal septation (Fig 3C and S5B, yellow arrows) and that 1% of the cells had adjacent septa which created mini-cell lacking DAPI-stained DNA (Fig 3C and Fig S5B, white arrows). We then analyzed by TEM the cell morphology and the structure of the septa for the WT, the Δ*prkC* mutant and the complemented strains. Cells with normal septation were observed for the WT strain, complemented strain and Δp*rkC* mutant (Fig 4A) while some cells of the Δ*prkC* mutant displayed aberrant septation with the presence of multiple and adjacent septa (Fig 4B). Mini-cells attached to each other were also observed (Fig 4B left) and these probably arise from the formation of several septa in close proximity (Fig 4B, right, red arrows). These results indicated that deletion of the *prkC* gene in *C. difficile* affects bacterial cell morphology and septum formation.

### *prkC* deletion increases sensitivity to detergents and autolysis

To determine if *prkC* deletion also affects the cell envelop, we tested the sensitivity of the *prkC* mutant to compounds with a detergent activity. The presence of 0.006% SDS affected the growth of the Δ*prkC* mutant but did not affect the WT and the complemented strains (Fig 5A). It is worth noting that in the gastrointestinal tract, *C. difficile* is subjected to the bactericidal effects of secondary bile salts that solubilize phospholipids, impair membrane integrity and weaken cell wall (48). We therefore tested the sensitivity of the Δ*prkC* mutant to the

454 secondary bile salt, deoxycholate (DOC) and to the primary bile salt, cholate. While the sen-
455 sitivity to cholate (0.03% or 0.04 % in TY) was similar for all the strains (data not shown),
456 we observed that the growth of the Δ*prkC* mutant was reduced in the presence of 0.03%
457 DOC (Fig 5B), a physiological concentration encountered in the gut (49, 50). In addition, the
458 autolysis in the presence of 0.01% of the non-ionic detergent Triton X-100 is more rapid for
459 the Δ*prkC* mutant than for the WT and the complemented strains (Fig 5C) while no differ-
460 ence in autolysis was observed in the absence of Triton (Fig S6A). This result suggested that
461 the Δ*prkC* mutant is more sensitive to the PG hydrolysis.
462
463 **PrkC controls sensitivity to antimicrobial compounds targeting the cell envelop**
464 Given that the deletion of *prkC* affected cell morphogenesis, we tested the sensitivity of the
465 *prkC* mutant to antibiotics targeting cell wall biosynthesis (46, 51). Using disk assays, we
466 showed that the size of the zone of inhibition increased for the Δ*prkC* mutant compared to
467 the WT and the complemented strains for all ß-lactams tested (Fig 6A). Thus, the *prkC* mu-
468 tant is more susceptible to ticarcillin, amoxicillin, imipenem and several cephalosporins
469 (cefoxitin, ceftazidime and cefepime). In contrast, we did not observe any differences for
470 antibiotics that target transcription or translation (Fig 6A and Fig S6B). We also observed an
471 important reduction in the MIC of the Δ*prkC* mutant compared to the WT strain for the gly-
472 copeptide, teicoplanin (>12-fold), but not for vancomycin (2-fold) (Table 1). In addition, we
473 observed a slight increase in the susceptibility of the mutant to amoxicillin and imipenem (4-
474 fold) and a more substantial increase for the cephalosporins tested (Table 1). The MIC for
475 the second-generation cephalosporin, cefoxitin, was reduced by more than 6-fold for the
476 Δ*prkC* mutant compared to the WT strain whereas the MIC for the third generation cephalo-
477 sporins, ceftazidime, cefepime and cefotaxime, was reduced for the Δ*prkC* mutant by 20-
478 17.5- and 8-fold, respectively. The same increase in sensitivity to cefoxitin, ceftazidine and
479 cefepime was seen for the Δ*prkC* mutant carrying pDIA6103-$P_{tet}$-*prkC*-K39→A (Fig 6A),
480 suggesting that the kinase activity of PrkC is required for *C. difficile* to express an intrinsic
481 high-level of resistance to cephalosporins (1).
482 Cationic antimicrobial peptides (CAMPs) that are produced by both bacteria and the host
483 also target the cell envelop and/or membrane of bacteria (52). Thus, we tested the resistance
484 of the WT and mutant strains for several CAMPS of bacterial origin. The MIC of the Δ*prkC*
485 mutant for polymixin B, bacitracin and nisin was 6-, 22- and 4.5-fold lower, respectively
486 than the MIC for the WT strain (Table 1). In the gastrointestinal tract, host-produced antimi-
487 crobial proteins such as lysozyme inhibit colonization of many Gram-positive pathogens by

hydrolyzing the PG and breaking the integrity of the cell wall. However, *C. difficile* is known for its intrinsic resistance to lysozyme that might be associated with high level of deacetylation of its PG (26). Interestingly, using an antimicrobial disk assay realized on Pep-M plates, we observed a greater size of the zone of inhibition for the Δ*prkC* mutant (17 mm) when compared to the WT strain (7.25 mm) in presence of 800 µg of lysozyme (Fig 6B). These results indicated that *prkC* deletion is involved in resistance to CAMPs and lysozyme.

**_prkC_ deletion affect motility, sedimentation and biofilm formation**

To identify other phenotypes associated with cell envelop properties, we first tested motility on semi-solid BHI plates and observed a reduced motility for the Δ*prkC* mutant compared to the WT and complemented strains (Fig 7A). After 48 h, the motility of the WT strain is 1.35 mm +/- 0.2 mm while the motility of the Δ*prkC* mutant is 0.8 mm +/- 0.1 mm. We also observed that the Δ*prkC* mutant formed more aggregates at the bottom of the tube than the WT and complemented strains (Fig S7A). We also tested the ability of these strains to form biofilm after an exposure to compounds triggering an envelope stress such as DOC or polymixin B. In the presence of sub-inhibitory concentration of polymixin B (20 µg/ml) or DOC (0.01%), the Δ*prkC* mutant formed, respectively, 6- and 10-fold more biofilm than the WT and complemented strains after 24 h, respectively (Fig 7B and C). However, no difference in biofilm formation was observed without these compounds (data not shown). When we quantified the biofilm formed in presence of DOC at 24 h, 48 h and 72 h (Fig S7B), we found that the Δ*prkC* mutant formed biofilm earlier than the WT strain (at 24 h) while more biofilm was produced by the WT strain than the Δ*prkC* mutant at 48 h. A previous work show that extracellular DNA (eDNA) is a major component of the matrix in DOC-induced biofilms (29). In both the Δ*prkC* mutant and the WT strain, DOC-induced biofilms were rapidly dispersed when treated with DNase (Fig S7C). Moreover, we detected eDNA in the extracellular matrix for the Δ*prkC* mutant at 24 h and 48 h but only at 48 h for the WT strain (Fig 7D). Since eDNA is required for biofilm stability (29), the early release of eDNA detected in the Δ*prkC* mutant might be responsible for the premature biofilm formation. Thus, deletion of *prkC* seems to affect the motility, the ability of *C. difficile* to sediment and to form biofilm under conditions that induce cell envelop stress.

**Comparison of the PG structure and composition between the WT strain and the Δ*prkC* mutant**

Based on the changes in cell-shape and increased susceptibility to ß-lactams and lysozyme of the Δ*prkC* mutant, we hypothesized that these phenotypes could be due to modification of the PG structure or composition. However, we showed that the muropeptide profiles of the WT strain (black) and the Δ*prkC* mutant (red) are almost identical (Fig S8). Indeed, we found no difference in the abundance of dimers containing a 3-3 cross-link (peaks 9, 10, 11, 13, 14, 15 and 17) generated by L,D-transpeptidases that might be associated with the high level of intrinsic resistance of *C. difficile* to some ß-lactams (31) or containing a 4-3 cross-link (peaks 18, 19, 21) catalyzed by D,D-transpeptidases, a target of ß-lactam (Fig S8). Moreover, the ratio of 4-3 to 3-3 cross-linking was not affected in our conditions. In addition, the amount of deacetylated muropeptides (peaks 4, 7, 9, 10, 11, 13, 14, 15, 17, 18, 19, 21) (31), was similar in the WT strain and the Δ*prkC* mutant (Fig S8). As muropeptides deacetylation contribute to a high level of resistance to lysozyme in *C. difficile* (26), the increased sensitivity of the Δ*prkC* mutant to lysozyme cannot be explained by changes in the level of PG deacetylation (Fig S8). Our results suggested that susceptibility of the *prkC* mutant to some ß-lactams or lysozyme is not related to changes of its PG structure or composition.

**Impact of the *prkC* deletion on the PSII**

In firmicutes, the wall teichoic acids (WTA) are involved in cell division, maintenance of cell-shape and susceptibility to CAMPs or ß-lactam (53). The 630Δ*erm* strain of *C. difficile* has an atypical wall teichoic acid known as polysaccharide II (PSII) composed of hexaglycosylphosphate repeats (34, 54). To know if the phenotypes observed for the Δ*prkC* mutant were associated with changes in the abundance, localization and/or structure of the PSII, we first purified the PSII of the WT and Δ*prkC* mutant strains. Their structure was analyzed by NMR and showed that the $^{1}$H NMR and $^{13}$C HSQC spectra from the 630Δ*erm* PSII were in good agreement with previous data (32, 54) and that no difference in the PSII structure was detected between the *prkC* mutant and the WT strain (Fig S9).

We also investigated a possible role for PrkC in controlling PSII localization. Using an immunoblot analysis with an antibody raised against PSII (34), we observed that more PSII was shed in the supernatant during growth by the Δ*prkC* mutant when compared to the parental and complemented strains during growth (Fig 8A). By contrast, we detected similar quantity of PSII in membrane fraction for all strains (Fig S10). Thus, this result suggests that the deletion of *prkC* leads to an enhanced release of PSII into the supernatant.

To precisely quantify the amount of PSII and PG in the cell wall of the WT and the Δ*prkC* mutant strains, we fractionated cells to recover the cell wall containing the PSII covalently linked to PG. We then separated these two compounds and quantified the amount of each product. Interestingly, we observed that the amount of PG purified from the Δ*prkC* mutant was lower compared to the WT strain, which represented 55 % of the quantity purified from the WT strain (Fig 8B). Similarly, but to a lesser extent, a reduction of 33 % in the quantity of PSII was observed for the Δ*prkC* mutant (Fig 8C). It is possible that the reduction in PG for the Δ*prkC* mutant could interfere with the localization of PSII and could explain the increase shedding of PSII in the supernatant (Fig 8A).

***prkC* deletion affects cell wall associated proteins**

Several properties of the bacterial cell envelop can be partly attributed to proteins localized at the cell surface. We extracted proteins non-covalently anchored to the cell wall of the Δ*prkC* mutant and the WT strains (55) and compared their relative abundance by mass spectrometry (Table 2 and Fig S11). A first family of proteins is the CWPs that contain a CWB2 motif responsible for their anchorage to the cell wall by interacting with PSII (56, 57). Indeed, we found that 27 CWP proteins with CWB2 (out of 29 in strain 630) including the S-layer protein, SlpA, were more abundant in the cell wall of the WT strain than in the Δ*prkC* mutant while a unique CWP protein, Cwp7, was more abundant in the Δ*prkC* mutant. Other non-covalently anchored proteins present of the cell surface (with SH3_3 or PG4 motifs) were also found in different amount in the WT strain and the Δ*prkC* mutant. Interestingly, some of them are involved in cell wall metabolism including L,D-transpeptidases, carboxypeptidases and putative cell wall hydrolases.

**Virulence and colonization of the Δ*prkC* mutant in the hamster model**

The different phenotypes of the *prkC* mutant suggest that PrkC can play a role during critical steps of the infectious cycle of *C. difficile* (4). To determine a possible role of PrkC in CDI, we compared the virulence of the WT strain and the Δ*prkC* mutant in the acute Golden Syrian hamster model of infection. Despite a trend towards a delay in the death of the hamsters infected with the *prkC* mutant, no significant difference was observed for the average time of post challenge survival between hamsters infected with the WT and the Δ*prkC* mutant strains (Fig 9A). When we monitored the daily level of gut colonization of the WT and the Δ*prkC* mutant, we found no significant difference in the average level of gut colonization the day the hamster died as determine by the average CFU per g of feces for each hamster (Fig

9B). However, a significant change in gut colonization was observed between the two strains 40 h post infection (Fig 9C). Despite the fact that the Δ*prkC* mutant has a delay in gut colonization, this delay has no significant effect on the virulence in this infection model.

**Discussion**

In this work, we showed that the *prkC* mutant of *C. difficile* has pleiotropic phenotypes such as an increased sensitivity to various antimicrobial compounds (CAMPs, lysozyme, DOC, ß-lactams), modifications in motility, cell aggregation and biofilm formation, and also changes in cell morphology and septum formation or localization. The increased sensitivity to several antimicrobial compounds detected for the *C. difficile* Δ*prkC* mutant has been observed in other firmicutes. The *prkA* mutant of *L. monocytogenes* is more sensitive to lysozyme and several CAMPs (58) while the *ireK* mutant of *E. faecalis* has an increased sensibility to bile and cholate (45) but not to DOC as observed for the *C. difficile* Δ*prkC* mutant. The inactivation of the PASTA-STKs in *S. pneumoniae*, *S. pyogenes*, *E. faecalis, L. monocytogenes* and *S. aureus* results in an increased susceptibility toward ß-lactams but the extent and pattern of the effects vary among species and strains (18, 45, 58, 59). These specific patterns of sensitivity observed for the PASTA-STK mutant for each firmicute might be associated with differences in the targets phosphorylated by the PASTA-STK, in the penicillin-binding proteins (PBPs) and in their affinity for the different ß-lactams. As observed in *B. subtilis* and *S. aureus* (18, 42), the PrkC kinase of *C. difficile* controls biofilm formation under cell-membrane stresses conditions. Several factors probably contribute to the increased biofilm formation in the Δ*prkC* mutant in the presence of DOC or polymixin B. This may include a decreased motility, an increased sedimentation and changes in the amount of CWPs that modify adhesive properties of the cell surface. For example, the Cwp84 protein, which is less abundant in the Δ*prkC* mutant is known to negatively control biofilm formation (60). In addition, premature autolysis by the Δ*prkC* mutant probably releases eDNA earlier in presence of DOC resulting in the increased biofilm formation observed at 24 h for the mutant (29). By controlling cell lysis, PrkC seems able to affect biofilm formation in response to cell membrane stresses.

Changes in the homeostasis and the integrity of the cell envelop might explain most of the phenotypes of the *C. difficile* Δ*prkC* mutant including modification of cell shape that is determined by the orderly processing and assembly of each cell wall component (53, 61, 62). The absence of PrkC probably modifies the abundance, composition and/or structure of component(s) of the cell envelop, including the PG, the glycopolymers (PSII and/or LTA-

622 PSIII) and/or cell-wall associated proteins (56). In other Gram-positive bacteria, PASTA-
623 STK phosphorylates enzymes involved in PG and/or teichoic acid synthesis, modification,
624 assembly and/or turnover. This includes enzymes of the Glm pathway, Mur enzymes, MviM,
625 a flippase involved in the transport of the lipid II anchored compounds across the membrane,
626 a penicillin-binding protein, LTA synthetases but also transcriptional regulators such as
627 WalR-WalK and GraR that control cell wall metabolism (17, 18, 63). In *C. difficile*, we did
628 not detect a transcriptional effect of the *prkC* deletion on genes encoding enzymes involved
629 in the synthesis of envelop components (E. Cuenot, unpublished data). These results strongly
630 suggest that PrkC does not act by modifying the activity of a transcriptional regulator but
631 rather by phosphorylating one or several protein(s) directly or indirectly controlling the syn-
632 thesis, assembly or turnover of at least one component of the envelop.
633 Teichoic acids play a role in protecting bacteria from stressful conditions by modifying
634 the properties of the cell surface. Changes in teichoic acids resulted in phenotypes similar to
635 those we observed in the Δ*prkC* mutant. This include increased ß-lactam susceptibility, au-
636 tolysis, modification of cell morphology and defect in septa positioning and numbers (53,
637 64). In *C. difficile*, the biosynthesis of the PSII, its properties as well as the phenotypes asso-
638 ciated with defect in PSII are poorly studied (32, 34). Furthermore, less information is avail-
639 able on atypical LTA (32). However, we noted that the Δ*prkC* mutant shares common phe-
640 notypes with the *lcpB* mutant encoding a protein involved in tethering PSII (34) that includes
641 elongated cell, presence of multiple septa and increased ability to form biofilms (34). While
642 the structure of PSII is not altered in the Δ*prkC* mutant, we observed a slightly reduction in
643 the amount of PSII anchored to the cell wall and an increased quantity in PSII released in the
644 supernatant of the Δ*prkC* mutant. These changes in PSII localization might be caused by the
645 dysregulation of PSII synthesis/anchorage or the production/assembly of another cell enve-
646 lope component such as PG in the absence of PrkC. Indeed, anchoring of the PSII to PG is
647 probably affected by the reduced amount of PG detected in the Δ*prkC* mutant.
648 As observed for *L. monocytogenes* and *E. faecalis, C. difficile* is inherently resistant to
649 cephalosporin and PASTA-STK inactivation leads to a robust increase in sensitivity towards
650 these antibiotics that target PG synthesis by inactivating PBPs (45, 65). In *C. difficile*, we
651 showed that the kinase activity of PrkC is required for the high level of resistance to cepha-
652 losporin. The sensitivity of the Δ*prkC* mutant to teicoplanin, an antibiotic that affects trans-
653 glycosylation by PBPs and to bacitracin that interferes with PG synthesis through its role on
654 lipid II recycling also suggests a possible role for this kinase in controlling PG metabolism
655 (66). Other phenotypes such as lysozyme resistance or autolysis are also related to PG struc-

ture or metabolism. However, we failed to detect any modification in the composition of PG, in reticulation of PG, 3-3 to 4-3 cross-link ratio or PG deacetylation under our experimental conditions. Changes to these would have offer, to a certain extent, an explanation for the increased sensitivity to cephalosporin and lysozyme. Nevertheless, it is possible that localized and/or subtle changes in PG composition occur at the septum, which is where PrkC is localized during growth. These changes would be difficult to detect. The main difference between the Δ*prkC* and the WT is a decrease in the total amount of PG. This might be linked to a reduced size of the glycan chains formed. It is interesting to note that proteins potentially involved in PG metabolism are also detected in different amount in the cell wall of the WT and Δ*prkC* mutant strains (Table 2). All these results suggest that PrkC has an effect directly or indirectly on PG synthesis or turnover in *C. difficile*. In *L. monocytogenes*, it has been suggested that the PASTA kinase might specifically regulate PBPs resulting in cephalosporin resistance(58). In *Enterococcus faecium,* mutants in class A PBPs are sensitive to cephalosporins and suppressor mutations that restore cephalosporin resistance are found in *ireK* and *ireP* encoding a STK and a STP, respectively (67). In *E. faecalis*, IreB negatively controls cephalosporin resistance and IreB is a small protein of unknown function and the only substrate of IreK kinase identified to date (68). However, the molecular mechanisms linking IreB, IreK and maybe PBPs that could explain their role in the control of cephalosporin resistance remain unknown. Interestingly, CD1283, the IreB-like protein of *C. difficile,* contains one threonine (T7) and this residue is phosphorylated in IreB of *E. faecalis*. CD1283 might contribute to the regulatory pathway downstream of PrkC. In addition, the PrkC-mediated phosphorylation of proteins controlling cell division and the synthesis of cell envelop components is another interesting hypothesis. Indeed, PrkC is localized at the septum and the deletion of the *prkC* gene affects *C. difficile* cell morphology with elongated cells, abnormal septum localization and defect in cell separation. In *S. pneumoniae* and other streptococci, Δ*stkP* mutants have longer cells than the WT and a modified shape and exhibits cell division and separation defects (69). Several proteins involved in cell division such as DivIVA, MapZ, GspB or FtsZ are phosphorylated by the PASTA-STKs in *B. subtilis*, *S. pneumoniae* or *S. aureus* (17, 18, 69). In *S. pneumoniae*, phosphorylation of DivIVA controls cell shape and the localization of PG synthesis machinery required for cell elongation and cell constriction (69). The phosphorylation by PrkC of an orthologous of one of these proteins, especially DivIVA, could explain several cell morphology associated phenotypes observed for the *prkC* mutant. Altogether, our results indicate that the PASTA-STK of *C.*

*difficile,* PrkC, is probably involved in the control of the envelop biogenesis and/or cell division.

Finally, the virulence of the Δ*prkC* mutant is similar to that of the WT strain while a colonization delay of the hamster gut is observed for the mutant. This can be explained by a global increased in sensitivity of the Δ*prkC* mutant to antimicrobial compounds and the possible changes in its cell envelop properties. Our results highlight the involvement of PrkC in controlling several processes corresponding to critical steps of CDI including resistance to DOC, known to inhibit growth of vegetative cells in the gastrointestinal tract (4), to lysozyme, a critical component of the innate immune system and to CAMPs produced by the microbiota and/or by the host (3) that are compounds present in the hamster model. Furthermore, dissecting the role of PrkC in controlling the resistance to antibiotics promoting CDI such as cephalosporins (1) could pave the way to new strategies for the prevention of these infections.

**Acknowledgments**.
We thank to Johann Peltier for helpful discussions and experimental advices, Gayatri Vedantam for the gift of the antibody raised against PSII, Jost Eninga for access to the fluorescent microscope, Nigel Minton for the genetic tools, Nicolas Kint for its help for the construction of the Δ*prkC* mutant and Sandrine Poncet for helpful advices. This work was funded by the Institut Pasteur, the University Paris 7, the ITN Marie Curie, Clospore (H2020-MSCA-ITN-2014 642068) and the ANR DifKin (ANR-17-CE15-0018-01). EC and TGG are the recipient of a ITN Marie Curie and an ANR fellowships, respectively.

**Table 1. MIC of the strain 630Δ*erm* and of the Δ*prkC* mutant for antibiotics targeting cell wall and CAMPS**

| Compound tested | MIC (µg/ml) | | Median-fold sensitization |
|---|---|---|---|
| | 630Δ*erm* | Δ*prkC* | |
| Antibiotics targeting cell wall | | | |
| Vancomycin | 1.5 | 0.75 | 2 |
| Teicoplanin | 0.19 | <0.016 | >12 |
| Amoxicillin | 4 | 1 | 4 |
| Imipenem | 6 | 1.3 | 4 |
| Cefoxitine | >256 | 44 | >6 |
| Ceftazidime | 60 | 3 | 20 |
| Cefepime | 70 | 4 | 17.5 |
| Cefotaxime | 128 | 16 | 8 |
| Antimicrobial peptides | | | |
| Polymixin B | 340 | 55 | 6 |
| Bacitracin | 550 | 25 | 22 |
| Nisin | 140 | 30 | 4.5 |

MICs for antibiotics were determined using E-test with the exception of cefotaxime.
The MICs for cefotaxime and antimicrobial peptides were determined by the method of dilution.

**Table 2. Change in cell wall associated proteins in *C. difficile* between the 630Δ*erm* strain and the Δ*prkC* mutant.**

| Gen ID | name | function | Fold-change 630Δerm/ Δ*prkC** | -Log (P-value) | Detected in surface proteome |
|---|---|---|---|---|---|
| **Cell-wall associated proteins CWB2 motif** | | | | | |
| Down in Δ*prkC* | | | | | |
| CD1233 | *cwp26* | Cell wall binding protein of skin element | 31.3 | 2.7 | |
| CD1469 | *cwp20* | Cell-wall penicillin-binding protein | 6.7 | 6.5 | |
| CD2518 | *cwp29* | Cell-wall binding protein | 6.4 | 4.6 | |
| CD2795 | *cwp11* | Cell-wall binding protein | 6.1 | 6.5 | |
| CD0440 | *cwp27* | Cell-wall binding protein | 5.1 | 4.3 | |
| CD2735 # | *cwp14* | Cell-wall binding protein (also SH3) | 4.8 | 5.2 | |
| CD2798 | *cwp9* | Cell-wall binding protein | 4.7 | 4.5 | |
| CD2767 | *cwp19* | Cell-wall binding protein, autolysin | 4.6 | 5.9 | |
| CD1803 | *cwp23* | Cell-wall binding protein | 4.4 | 4.9 | |
| CD2786 | *cwp5* | Cell-wall binding protein | 4.4 | 5.4 | |
| CD1751 | *cwp13* | Cell-wall binding protein, protease | 4.2 | 5.4 | |
| CD2787 | *cwp84* | Cell-wall binding protein, protease | 4.0 | 5.4 | + |
| CD2193 | *cwp24* | Cell-wall binding protein, glucosaminidase domain | 3.9 | 4.4 | + |
| CD0844 | *cwp25* | Cell-wall binding protein | 3.9 | 5.9 | + |
| CD3192 | *cwp21* | Cell-wall binding protein | 3.9 | 6.8 | |
| CD2789 | *cwp66* | Cell-wall binding protein | 3.8 | 4.7 | |
| CD2791 | *cwp2* | Cell-wall binding protein | 3.7 | 6.6 | + |
| CD2793 | *slpA* | Precursor of the S-layer proteins | 3.6 | 4.90 | + |
| CD2713 # | *ldtcd2, cwp22* | Cell-wall binding protein, L,D-transpeptidases | 3.6 | 5.1 | |
| CD2794 | *cwp12* | Cell-wall binding protein | 3.6 | 5.6 | |
| CD0514 | *cwpV* | Hemagglutinin/adhesin | 3.4 | 4.8 | + |
| CD1987 | *cwp28* | Cell-wall binding protein | 3.1 | 1.5 | |
| CD1035 | *cwp16* | Cell-wall binding protein, amidase domain | 3.1 | 5.7 | |
| CD1036 | *cwp17* | Cell-wall binding protein, amidase domain | 2.9 | 3.3 | |
| CD2796 | *cwp10* | Cell-wall binding protein | 2.8 | 4.8 | |
| CD2784 | *cwp6* | Cell-wall binding protein, amidase domain | 2.8 | 3.6 | + |
| CD1047 | *cwp18* | Cell-wall binding protein | 2.4 | 3.5 | |
| CD2799 | *cwp8* | Cell-wall binding protein | 2.1 | 4.0 | |
| **Up in Δ*prkC*** | | | | | |
| CD2782 | *cwp7* | Cell-wall binding protein | 0.2 | 2.1 | |
| **SH3_3 motif** | | | | | |
| Down in Δ*prkC* | | | | | |
| CD0183 # | | Putative cell-wall hydrolase | 10.2 | 1 | |
| CD2768 # | | Putative cell-wall hydrolase | 3.8 | 2.9 | |
| CD1135 # | | Putative endopeptidase | 3 | 4.8 | |
| CD2402 # | | Putative cell wall hydrolase phosphatase-associated protein | 2.3 | 2.6 | |
| **PG4 motif** | | | | | |

| | | | | | |
|---|---|---|---|---|---|
| Up in Δ*prkC* | | | | | |
| CD1436 | | Putative hydrolase^ | 0.2 | 2.4 | |
| CD2963# | *ldtcd1* | L,D-transpeptidases^ | 0.3 | 2.5 | |
| CD2149 | | Putative vancomycin resistance protein, VanW family^ | 0.3 | 1.1 | |

# cell wall metabolism
*FDR<0.05
^protein containing one trans-membrane domain
SH3 domain (PF08239), CWB 2 motif (PD04122) and PG4 motif (PF12229)

## Figure Legend

**Figure 1. Organization, localization and kinase activity of the PrkC protein.**
A. Organization of the domains of *C. difficile* CD2578-PrkC. PrkC contains a cytoplasmic kinase domain in N-terminal part (brown), a trans-membrane (TM) segment, two PASTA domains (green) and an atypical SGN (Ser, Gly, Asn) rich domain in C-terminal part (pink). The conserved lysine residue (K39) within the ATP-binding P loop of the kinase that is required for phosphotransfer is indicated.
B. Localization of the PrkC-HA tagged protein. Cells expressing *prkC* fused to HA were grown in the presence of 15 ng/ml of ATc, and harvested during exponential growth. Samples were fractionated into membrane (Mb) and cytoplasm (Cy) fractions. Protein fractions were analyzed by western blot using an antibody raised against HA.
C. Localization of the SNAP-PrkC fusion during growth. The SNAP-PrkC protein was produced during exponential growth phase in the presence of 50 ng/ml ATc. After labeling with the TMR-star substrate, PrkC-SNAP localization was analyzed by fluorescence microscopy. AF (autofluorescence). The scale bar represents 5 μm.
D. Western blot performed after fractionation in a soluble fraction (1) and an insoluble fraction (2) obtained from exponential phase cultures of the WT, the Δ*prkC* mutant, the complemented strain and the Δ*prkC* mutant carrying pDIA6103-*prkC*-K39→A (K→A). An α-P-Thr antibody was used to detect phosphorylated threonine. We indicated by red arrows the bands detected in the WT strain that disappeared in the Δ*prkC* mutant.

**Figure 2. Genetic organization of the *prkC* locus**
A. Schematic representation of the gene cluster present upstream of *prkC*. The locus between *CD2590-dapF* and *prkC* includes genes encoding proteins involved in translation, transcription, DNA replication, metabolism and membrane proteins. The genome-wide TSS mapping (25) indicated the presence of a promoter upstream of *dapF*. The extended -10 box and the TSS are indicated in bold.
B. PCR realized with primers annealing in *prkC* and *stp* (IMV936 and IMV908, line 1 and 2) or *stp* and *rlmN* (IMV935 and IMV907, line 3 and 4) either on RNA extracted from 630Δ*erm* (line 1 and 3) or on cDNA synthesized by reverse transcription from the same RNA using primer IMV843 (line 2 and 4). Smart Ladder (200-10,000 bp).

**Figure 3. Morphology of the Δ*prkC* mutant**
A. Fluorescence microscopy was carried out on the WT, the Δ*prkC* mutant and the complemented (Comp) strains. Membranes and DNA were visualized with FM4-64 (red) and DAPI (blue), respectively. A blue arrow showed an elongated cell and green arrows non-separated cells. The white square indicates the presence of a septum with an aberrant structure. Scale bars represent 5 μm.

B. Cell size distribution for the WT, the Δ*prkC* mutant and the complemented (Comp) strains. The measurement was done on cells labeled with FM4-64 and DAPI. Means and errors of the means were calculated after the measurement of at least 600 cells for each strain. The analysis was performed with the software Imaje J.
C. Presence of aberrant septation and anucleated minicells in *ΔprkC* mutant cells. Fluorescence microscopy of cells staining with FM4-64 and DAPI revealed the presence of aberrant septum (yellow arrows) and anucleate minicells (white arrows) in the Δ*prkC* mutant. Scale bars represent 5 µm.

**Figure 4. Presence of abnormal septa in the Δ*prkC* mutant cells**
A. TEM pictures showing normal septal structure in the 630Δ*erm* (WT), the Δ*prkC* mutant and the complemented (Comp) strains. Scale bars represent 100 nm.
B. TEM pictures showing aberrant septal structure in the Δ*prkC* mutant cells. In the right panel, we can distinguish the beginning of the synthesis of two septa (white arrows) has begun near an apparent normal septum. Scale bars represent 200 nm.

**Figure 5. *prkC* deletion increases sensitivity to detergents and autolysis**
A. Resistance to SDS stress of the Δ*prkC* mutant, the 630Δ*erm* (WT) and the complement strains (Comp) was tested on BHI plates containing 0.006 % of SDS. This experiment was performed in triplicate and this plate is representative of the results obtained.
B. Growth of the WT strain (black circle), the Δ*prkC* mutant (white circle) and the complemented strain (white square) in 24-well microplates containing TY medium in the presence of 0.03% DOC. A growth curve without DOC is presented in Fig S3. 4 independent cultures were done.
C. Autolysis of the WT (black circle), Δ*prkC* (white circle) and complemented (black square) strains in the presence of 0.01% Triton X-100. The $OD_{600nm}$ of the samples incubated at 37°C was determined every 5 min until complete cell lysis was reached. 4 independent experiments were done.

**Figure 6. Sensitivity of the Δ*prkC* mutant to antibiotics targeting cell-wall and to lysozyme.**
A. Sensitivity to antibiotics targeting the cell wall. Histograms representing the diameters of growth inhibition area after 24 h of incubation on BHI plates for the 630Δ*erm* strain pDIA6103 (WT, black), the Δ*prkC* mutant pDIA6103 (medium grey), the complemented strain (Comp, dark grey) and the Δ*prkC* mutant expressing PrkC-K39A (pale grey). We used antibiogram disks containing Ticarcillin 75 µg, Amoxicillin 25 µg, Imipenem 10 µg, Ceftazidime 30 µg, Cefepime 30 µg or Erythromycin 15 µg. Cefoxitin was tested at 100 µg. The results presented correspond to 7 experiments (Ticarcillin, Amoxicillin, Imipenem) or 4 experiments for cephalosporins. Data were analyzed by t test. * indicates $P<0.05$.
B. Sensitivity to lysozyme was determined on Pep-M plates. 800 µg of lysozyme was added to a 6-mm disk. Histograms representing the diameter of growth inhibition measured for the 630Δ*erm* pDIA6103 (WT, black), the Δ*prkC* mutant pDIA6103 (medium grey), and the complemented strain (Comp, dark grey). The experiment was performed in quadruplicate. Data were analyzed by t test. * indicates $P<0.05$.

**Figure 7. Sedimentation, biofilm formation and motility of the Δ*prkC* mutant**
A. Motility test on 0.3% agar BHI plates. The plates shown are representatives of 3 independent tests.
B and C Mean values of the $OD_{570nm}$ measured after crystal violet staining of the mass of biofilm obtained after 24 h in presence of 20 µM polymixin B (B) or 0.01% DOC (C). Error

bars show standard deviation of three independent experiments performed in triplicate. Data were analyzed by t test. P values were 0.031 and 0.0045 for polymixin B (B) and DOC (C), respectively. On the picture, crystal violet staining revealing the amount of biofilm formed after 24 h corresponding to the values represented above.
D. Detection of e-DNA in the matrix of 24 h and 48 h DOC-induced biofilms formed by the WT strain and the Δ*prkC* mutant. The experience was done in triplicate. We presented a gel representative of the results obtained.

**Figure 8. Impact of *prkC* deletion on PSII localization and PG and PSII production**
A. Immunoblot detection of PSII using a serum antibody raised against this glycopolymer (34) in supernatants of the WT, Δ*prkC* and complemented strains. For each sample, we normalized by using the $OD_{600nm}$ of the corresponding culture. ND, not diluted. All immunoblots are representative of at least four replicates.
B and C. Quantification of the PG (B) and PSII (C) present at the surface of the WT and the Δ*prkC* mutant strains. The values were normalized to the WT levels considered as 1. Error bars represents standard deviation of at least 4 independent experiments.

**Figure 9. *prkC* deletion affect gut establishment and not virulence**
A. Average survival time (h) post-infection for hamsters challenged with 630Δ*erm* or Δ*prkC* spores.
B and C. Average quantity of CFU per g of feces determined the day of animal death (B) or 40 h post infection (C) for hamsters challenged with 630Δ*erm* or Δ*prkC* spores. The average values (B) were calculated with 16 and 12 hamsters for the WT strain and the Δ*prkC* mutant, respectively due to the absence of feces at this time point for four hamsters.
The average values (C) were calculated with the totality of hamsters for both groups. Data were analyzed by a Mann-Whitney test. * indicates $P<0.05$. The sensitivity threshold of the method is $10^3$ g/feces.

**References**


1. **Spigaglia P.** 2016. Recent advances in the understanding of antibiotic resistance in *Clostridium difficile* infection. Ther Adv Infect Dis **3:**23-42.
2. **Smits WK, Lyras D, Lacy DB, Wilcox MH, Kuijper EJ.** 2016. *Clostridium difficile* infection. Nat Rev Dis Primers **2:**16020.
3. **Abt MC, McKenney PT, Pamer EG.** 2016. *Clostridium difficile* colitis: pathogenesis and host defence. Nat Rev Microbiol **14:**609-620.
4. **Sorg JA.** 2014. Microbial bile acid metabolic clusters: the bouncers at the bar. Cell Host Microbe **16:**551-552.
5. **Pantaleon V, Bouttier S, Soavelomandroso AP, Janoir C, Candela T.** 2014. Biofilms of Clostridium species. Anaerobe **30:**193-198.
6. **Paredes-Sabja D, Shen A, Sorg JA.** 2014. *Clostridium difficile* spore biology: sporulation, germination, and spore structural proteins. Trends Microbiol **22:**406-416.
7. **Janoir C.** 2016. Virulence factors of *Clostridium difficile* and their role during infection. Anaerobe **37:**13-24.
8. **Toth M, Stewart NK, Smith C, Vakulenko SB.** 2018. Intrinsic Class D beta-Lactamases of *Clostridium difficile*. MBio **9**.

9. **Kint N, Janoir C, Monot M, Hoys S, Soutourina O, Dupuy B, Martin-Verstraete I.** 2017. The alternative sigma factor sigma(B) plays a crucial role in adaptive strategies of *Clostridium difficile* during gut infection. Environ Microbiol **19:**1933-1958.
10. **Pereira SF, Goss L, Dworkin J.** 2011. Eukaryote-like serine/threonine kinases and phosphatases in bacteria. Microbiol Mol Biol Rev **75:**192-212.
11. **Dworkin J.** 2015. Ser/Thr phosphorylation as a regulatory mechanism in bacteria. Curr Opin Microbiol **24:**47-52.
12. **Jers C, Soufi B, Grangeasse C, Deutscher J, Mijakovic I.** 2008. Phosphoproteomics in bacteria: towards a systemic understanding of bacterial phosphorylation networks. Expert Rev Proteomics **5:**619-627.
13. **Pompeo F, Foulquier E, Galinier A.** 2016. Impact of Serine/Threonine Protein Kinases on the Regulation of Sporulation in *Bacillus subtilis*. Front Microbiol **7:**568.
14. **Maestro B, Novakova L, Hesek D, Lee M, Leyva E, Mobashery S, Sanz JM, Branny P.** 2011. Recognition of peptidoglycan and beta-lactam antibiotics by the extracellular domain of the Ser/Thr protein kinase StkP from *Streptococcus pneumoniae*. FEBS Lett **585:**357-363.
15. **Squeglia F, Marchetti R, Ruggiero A, Lanzetta R, Marasco D, Dworkin J, Petoukhov M, Molinaro A, Berisio R, Silipo A.** 2011. Chemical basis of peptidoglycan discrimination by PrkC, a key kinase involved in bacterial resuscitation from dormancy. J Am Chem Soc **133:**20676-20679.
16. **Hardt P, Engels I, Rausch M, Gajdiss M, Ulm H, Sass P, Ohlsen K, Sahl HG, Bierbaum G, Schneider T, Grein F.** 2017. The cell wall precursor lipid II acts as a molecular signal for the Ser/Thr kinase PknB of *Staphylococcus aureus*. Int J Med Microbiol **307:**1-10.
17. **Manuse S, Fleurie A, Zucchini L, Lesterlin C, Grangeasse C.** 2016. Role of eukaryotic-like serine/threonine kinases in bacterial cell division and morphogenesis. FEMS Microbiol Rev **40:**41-56.
18. **Pensinger DA, Schaenzer AJ, Sauer JD.** 2017. Do Shoot the Messenger: PASTA Kinases as Virulence Determinants and Antibiotic Targets. Trends Microbiol doi:10.1016/j.tim.2017.06.010.
19. **Banu LD, Conrads G, Rehrauer H, Hussain H, Allan E, van der Ploeg JR.** 2010. The *Streptococcus mutans* serine/threonine kinase, PknB, regulates competence development, bacteriocin production, and cell wall metabolism. Infect Immun **78:**2209-2220.
20. **Ng YK, Ehsaan M, Philip S, Collery MM, Janoir C, Collignon A, Cartman ST, Minton NP.** 2013. Expanding the repertoire of gene tools for precise manipulation of the *Clostridium difficile* genome: allelic exchange using pyrE alleles. PLoS One **8:**e56051.
21. **Wilson KH, Kennedy MJ, Fekety FR.** 1982. Use of sodium taurocholate to enhance spore recovery on a medium selective for *Clostridium difficile*. J Clin Microbiol **15:**443-446.
22. **Dembek M, Stabler RA, Witney AA, Wren BW, Fairweather NF.** 2013. Transcriptional analysis of temporal gene expression in germinating *Clostridium difficile* 630 endospores. PLoS One **8:**e64011.
23. **Fagan RP, Fairweather NF.** 2011. *Clostridium difficile* has two parallel and essential Sec secretion systems. J Biol Chem **286:**27483-27493.

24. **Cartman ST, Kelly ML, Heeg D, Heap JT, Minton NP.** 2012. Precise manipulation of the *Clostridium difficile* chromosome reveals a lack of association between the *tcdC* genotype and toxin production. Appl Environ Microbiol **78:**4683-4690.
25. **Soutourina OA, Monot M, Boudry P, Saujet L, Pichon C, Sismeiro O, Semenova E, Severinov K, Le Bouguenec C, Coppee JY, Dupuy B, Martin-Verstraete I.** 2013. Genome-wide identification of regulatory RNAs in the human pathogen *Clostridium difficile*. PLoS Genet **9:**e1003493.
26. **Ho TD, Williams KB, Chen Y, Helm RF, Popham DL, Ellermeier CD.** 2014. *Clostridium difficile* extracytoplasmic function sigma factor sigmaV regulates lysozyme resistance and is necessary for pathogenesis in the hamster model of infection. Infect Immun **82:**2345-2355.
27. **McBride SM, Sonenshein AL.** 2011. The dlt operon confers resistance to cationic antimicrobial peptides in *Clostridium difficile*. Microbiology **157:**1457-1465.
28. **Saujet L, Monot M, Dupuy B, Soutourina O, Martin-Verstraete I.** 2011. The key sigma factor of transition phase, SigH, controls sporulation, metabolism, and virulence factor expression in *Clostridium difficile*. J Bacteriol **193:**3186-3196.
29. **Dubois T, Tremblay Y, Hamiot A, Martin-Verstraete I, Deschamps J, Monot M, Briandet B, Dupuy B.** 2018. A microbiota-generated bile salt induces biofilm formation in *Clostridium difficile*. in revision.
30. **Schneider CA, Rasband WS, Eliceiri KW.** 2012. NIH Image to ImageJ: 25 years of image analysis. Nat Methods **9:**671-675.
31. **Peltier J, Courtin P, El Meouche I, Lemee L, Chapot-Chartier MP, Pons JL.** 2011. *Clostridium difficile* has an original peptidoglycan structure with a high level of N-acetylglucosamine deacetylation and mainly 3-3 cross-links. J Biol Chem **286:**29053-29062.
32. **Reid CW, Vinogradov E, Li J, Jarrell HC, Logan SM, Brisson JR.** 2012. Structural characterization of surface glycans from *Clostridium difficile*. Carbohydr Res **354:**65-73.
33. **Candela T, Fouet A.** 2005. *Bacillus anthracis* CapD, belonging to the gamma-glutamyltranspeptidase family, is required for the covalent anchoring of capsule to peptidoglycan. Mol Microbiol **57:**717-726.
34. **Chu M, Mallozzi MJ, Roxas BP, Bertolo L, Monteiro MA, Agellon A, Viswanathan VK, Vedantam G.** 2016. A *Clostridium difficile* Cell Wall Glycopolymer Locus Influences Bacterial Shape, Polysaccharide Production and Virulence. PLoS Pathog **12:**e1005946.
35. **Lago M, Monteil V, Douche T, Guglielmini J, Criscuolo A, Maufrais C, Matondo M, Norel F.** 2017. Proteome remodelling by the stress sigma factor RpoS/sigma(S) in Salmonella: identification of small proteins and evidence for post-transcriptional regulation. Sci Rep **7:**2127.
36. **Cox J, Mann M.** 2008. MaxQuant enables high peptide identification rates, individualized p.p.b.-range mass accuracies and proteome-wide protein quantification. Nat Biotechnol **26:**1367-1372.
37. **Cox J, Neuhauser N, Michalski A, Scheltema RA, Olsen JV, Mann M.** 2011. Andromeda: a peptide search engine integrated into the MaxQuant environment. J Proteome Res **10:**1794-1805.

38. **Tyanova S, Temu T, Sinitcyn P, Carlson A, Hein MY, Geiger T, Mann M, Cox J.** 2016. The Perseus computational platform for comprehensive analysis of (prote)omics data. Nat Methods **13:**731-740.
39. **Tusher VG, Tibshirani R, Chu G.** 2001. Significance analysis of microarrays applied to the ionizing radiation response. Proc Natl Acad Sci U S A **98:**5116-5121.
40. **Vizcaino JA, Csordas A, del-Toro N, Dianes JA, Griss J, Lavidas I, Mayer G, Perez-Riverol Y, Reisinger F, Ternent T, Xu QW, Wang R, Hermjakob H.** 2016. 2016 update of the PRIDE database and its related tools. Nucleic Acids Res **44:**D447-456.
41. **Huse M, Kuriyan J.** 2002. The conformational plasticity of protein kinases. Cell **109:**275-282.
42. **Madec E, Laszkiewicz A, Iwanicki A, Obuchowski M, Seror S.** 2002. Characterization of a membrane-linked Ser/Thr protein kinase in *Bacillus subtilis*, implicated in developmental processes. Mol Microbiol **46:**571-586.
43. **Morlot C, Bayle L, Jacq M, Fleurie A, Tourcier G, Galisson F, Vernet T, Grangeasse C, Di Guilmi AM.** 2013. Interaction of Penicillin-Binding Protein 2x and Ser/Thr protein kinase StkP, two key players in *Streptococcus pneumoniae* R6 morphogenesis. Mol Microbiol **90:**88-102.
44. **Iwanicki A, Hinc K, Seror S, Wegrzyn G, Obuchowski M.** 2005. Transcription in the prpC-yloQ region in *Bacillus subtilis*. Arch Microbiol **183:**421-430.
45. **Kristich CJ, Wells CL, Dunny GM.** 2007. A eukaryotic-type Ser/Thr kinase in *Enterococcus faecalis* mediates antimicrobial resistance and intestinal persistence. Proc Natl Acad Sci U S A **104:**3508-3513.
46. **Kristich CJ, Little JL, Hall CL, Hoff JS.** 2011. Reciprocal regulation of cephalosporin resistance in *Enterococcus faecalis*. MBio **2:**e00199-00111.
47. **Shah IM, Laaberki MH, Popham DL, Dworkin J.** 2008. A eukaryotic-like Ser/Thr kinase signals bacteria to exit dormancy in response to peptidoglycan fragments. Cell **135:**486-496.
48. **Hofmann AF, Hagey LR.** 2008. Bile acids: chemistry, pathochemistry, biology, pathobiology, and therapeutics. Cell Mol Life Sci **65:**2461-2483.
49. **Northfield TC, McColl I.** 1973. Postprandial concentrations of free and conjugated bile acids down the length of the normal human small intestine. Gut **14:**513-518.
50. **Ridlon JM, Kang DJ, Hylemon PB.** 2006. Bile salt biotransformations by human intestinal bacteria. J Lipid Res **47:**241-259.
51. **Beltramini AM, Mukhopadhyay CD, Pancholi V.** 2009. Modulation of cell wall structure and antimicrobial susceptibility by a *Staphylococcus aureus* eukaryote-like serine/threonine kinase and phosphatase. Infect Immun **77:**1406-1416.
52. **Nawrocki KL, Crispell EK, McBride SM.** 2014. Antimicrobial Peptide Resistance Mechanisms of Gram-Positive Bacteria. Antibiotics (Basel) **3:**461-492.
53. **Brown S, Santa Maria JP, Jr., Walker S.** 2013. Wall teichoic acids of gram-positive bacteria. Annu Rev Microbiol **67:**313-336.
54. **Ganeshapillai J, Vinogradov E, Rousseau J, Weese JS, Monteiro MA.** 2008. *Clostridium difficile* cell-surface polysaccharides composed of pentaglycosyl and hexaglycosyl phosphate repeating units. Carbohydr Res **343:**703-710.
55. **Laemmli UK.** 1970. Cleavage of structural proteins during the assembly of the head of bacteriophage T4. Nature **227:**680-685.
56. **Kirk JA, Banerji O, Fagan RP.** 2017. Characteristics of the *Clostridium difficile* cell envelope and its importance in therapeutics. Microb Biotechnol **10:**76-90.

57. **Willing SE, Candela T, Shaw HA, Seager Z, Mesnage S, Fagan RP, Fairweather NF.** 2015. *Clostridium difficile* surface proteins are anchored to the cell wall using CWB2 motifs that recognise the anionic polymer PSII. Mol Microbiol **96:**596-608.
58. **Pensinger DA, Boldon KM, Chen GY, Vincent WJ, Sherman K, Xiong M, Schaenzer AJ, Forster ER, Coers J, Striker R, Sauer JD.** 2016. The *Listeria monocytogenes* PASTA Kinase PrkA and Its Substrate YvcK Are Required for Cell Wall Homeostasis, Metabolism, and Virulence. PLoS Pathog **12:**e1006001.
59. **Dias R, Felix D, Canica M, Trombe MC.** 2009. The highly conserved serine threonine kinase StkP of *Streptococcus pneumoniae* contributes to penicillin susceptibility independently from genes encoding penicillin-binding proteins. BMC Microbiol **9:**121.
60. **Pantaleon V, Soavelomandroso AP, Bouttier S, Briandet R, Roxas B, Chu M, Collignon A, Janoir C, Vedantam G, Candela T.** 2015. The *Clostridium difficile* Protease Cwp84 Modulates both Biofilm Formation and Cell-Surface Properties. PLoS One **10:**e0124971.
61. **Siegel SD, Liu J, Ton-That H.** 2016. Biogenesis of the Gram-positive bacterial cell envelope. Curr Opin Microbiol **34:**31-37.
62. **Typas A, Banzhaf M, Gross CA, Vollmer W.** 2011. From the regulation of peptidoglycan synthesis to bacterial growth and morphology. Nat Rev Microbiol **10:**123-136.
63. **Pompeo F, Rismondo J, Grundling A, Galinier A.** 2018. Investigation of the phosphorylation of *Bacillus subtilis* LTA synthases by the serine/threonine kinase PrkC. Sci Rep **8:**17344.
64. **Percy MG, Grundling A.** 2014. Lipoteichoic acid synthesis and function in gram-positive bacteria. Annu Rev Microbiol **68:**81-100.
65. **Pensinger DA, Aliota MT, Schaenzer AJ, Boldon KM, Ansari IU, Vincent WJ, Knight B, Reniere ML, Striker R, Sauer JD.** 2014. Selective pharmacologic inhibition of a PASTA kinase increases *Listeria monocytogenes* susceptibility to beta-lactam antibiotics. Antimicrob Agents Chemother **58:**4486-4494.
66. **Eggert US, Ruiz N, Falcone BV, Branstrom AA, Goldman RC, Silhavy TJ, Kahne D.** 2001. Genetic basis for activity differences between vancomycin and glycolipid derivatives of vancomycin. Science **294:**361-364.
67. **Desbonnet C, Tait-Kamradt A, Garcia-Solache M, Dunman P, Coleman J, Arthur M, Rice LB.** 2016. Involvement of the Eukaryote-Like Kinase-Phosphatase System and a Protein That Interacts with Penicillin-Binding Protein 5 in Emergence of Cephalosporin Resistance in Cephalosporin-Sensitive Class A Penicillin-Binding Protein Mutants in *Enterococcus faecium*. MBio **7:**e02188-02115.
68. **Hall CL, Tschannen M, Worthey EA, Kristich CJ.** 2013. IreB, a Ser/Thr kinase substrate, influences antimicrobial resistance in *Enterococcus faecalis*. Antimicrob Agents Chemother **57:**6179-6186.
69. **Fleurie A, Cluzel C, Guiral S, Freton C, Galisson F, Zanella-Cleon I, Di Guilmi AM, Grangeasse C.** 2012. Mutational dissection of the S/T-kinase StkP reveals crucial roles in cell division of *Streptococcus pneumoniae*. Mol Microbiol **83:**746-758.

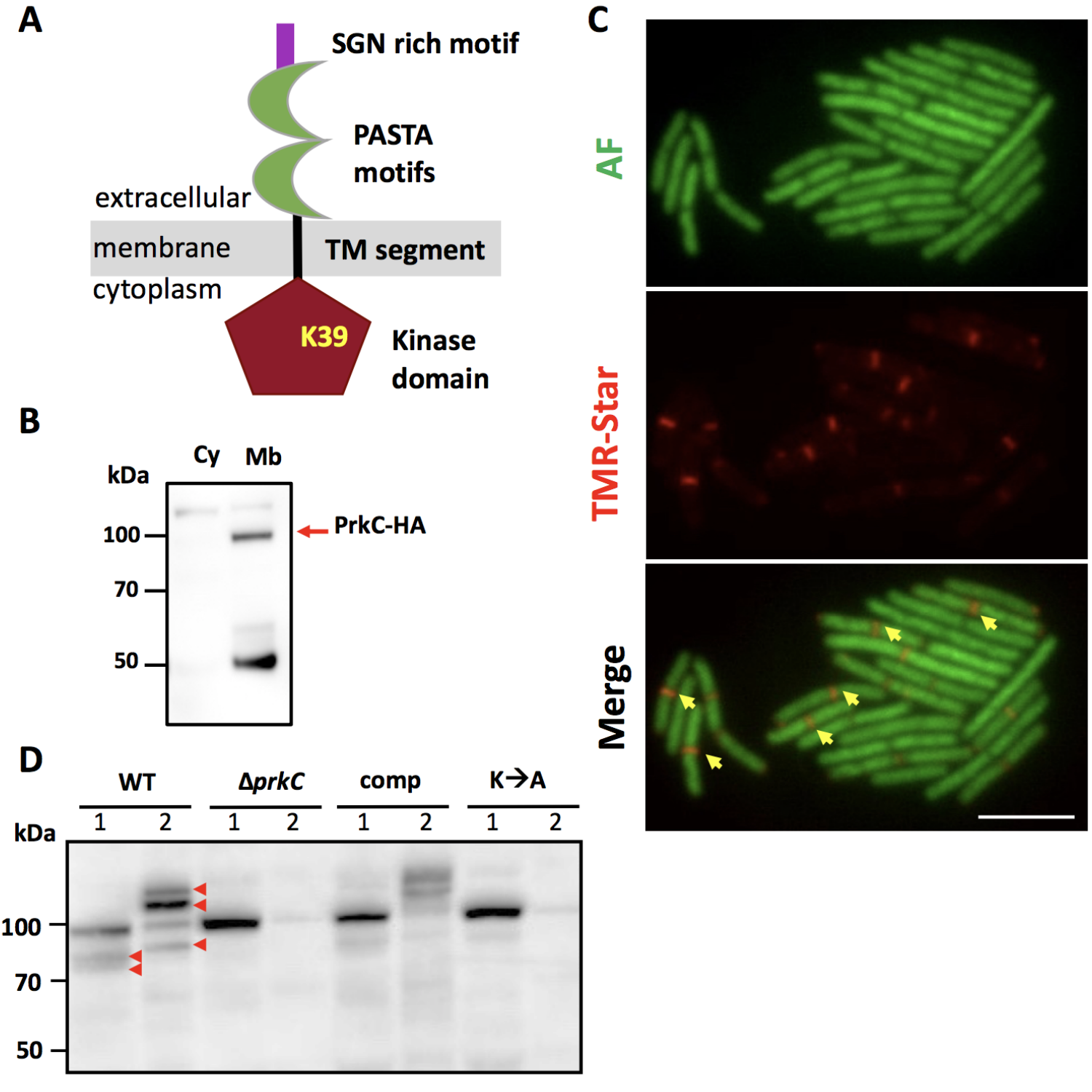
A
SGN rich motif
PASTA motifs
extracellular
membrane
TM segment
cytoplasm
K39
Kinase domain
B
Cy
Mb
kDa
100
70
50
PrkC-HA
C
AF
TMR-Star
Merge
D
WT
ΔprkC
comp
K→A
1
2
kDa
100
70
50

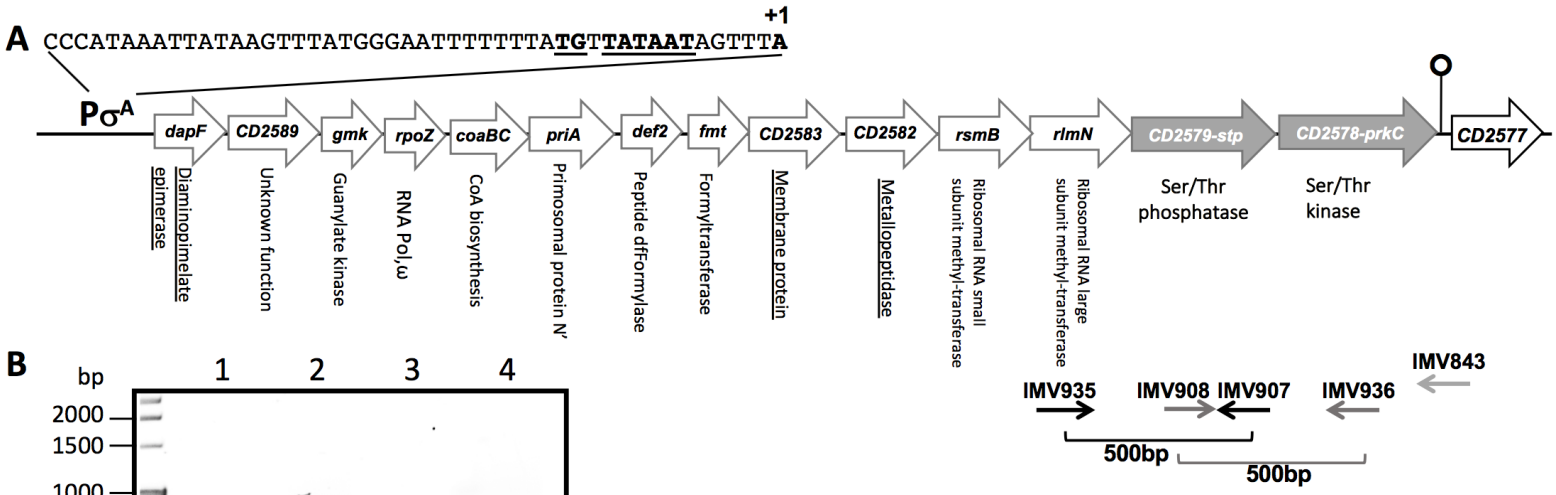
A
CCCATAAATTATAAGTTTATGGGAATTTTTTTATGTTATAATAGTTTA
+1
PσA
dapF
CD2589
gmk
rpoZ
coaBC
priA
def2
fmt
CD2583
CD2582
rsmB
rlmN
CD2579-stp
CD2578-prkC
CD2577
Diaminopimelate epimerase
Unknown function
Guanylate kinase
RNA Pol,ω
CoA biosynthesis
Primosomal protein N'
Peptide dfFormylase
Formyltransferase
Membrane protein
Metallopeptidase
Ribosomal RNA small subunit methyl-transferase
Ribosomal RNA large subunit methyl-transferase
Ser/Thr phosphatase
Ser/Thr kinase
B
bp
1
2
3
4
2000
1500
1000
800
600
400
200
IMV935
IMV908
IMV907
IMV936
IMV843
500bp
500bp

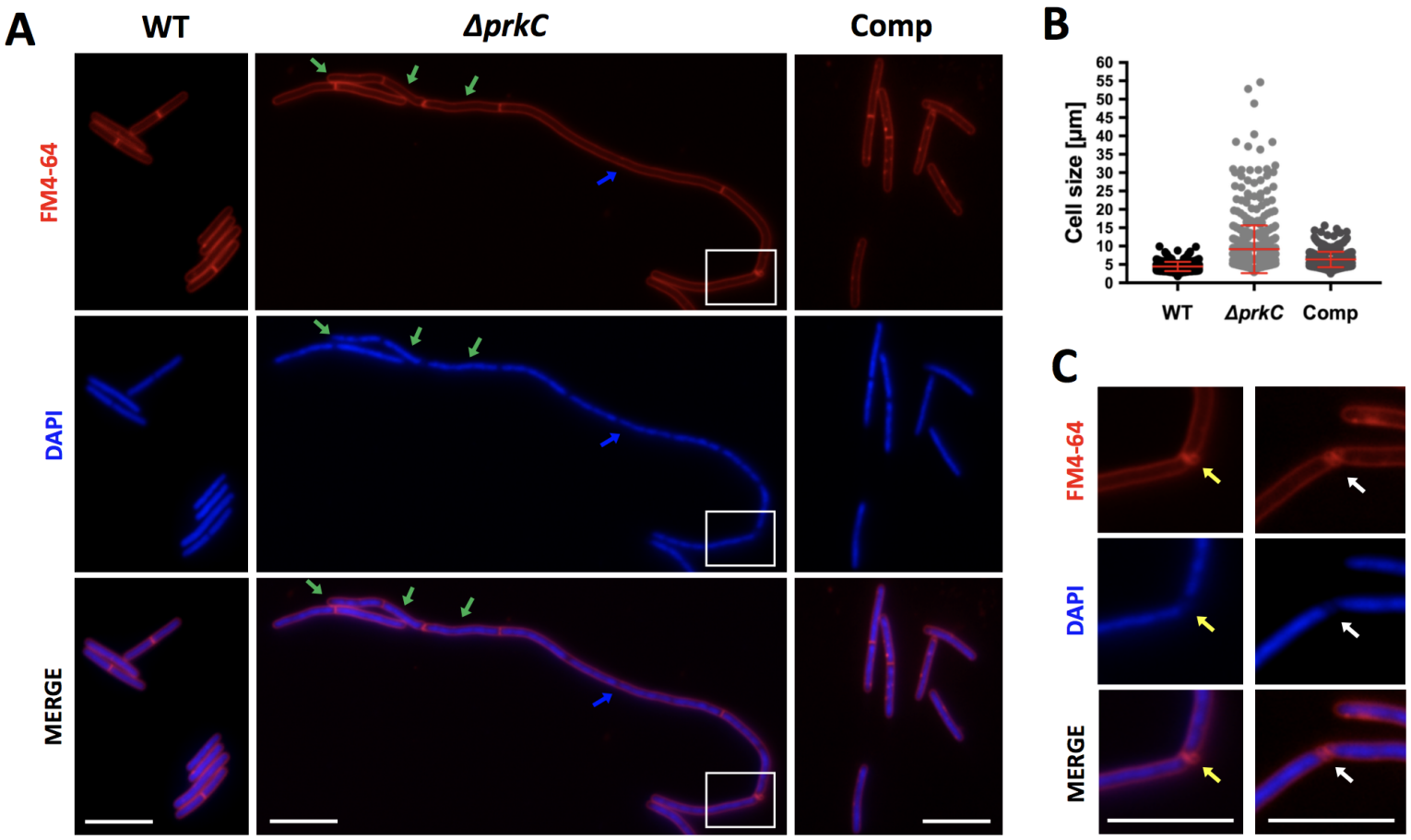
A
WT
ΔprkC
Comp
FM4-64
DAPI
MERGE
B
Cell size [µm]
60
55
50
45
40
35
30
25
20
15
10
5
0
WT
ΔprkC
Comp
C
FM4-64
DAPI
MERGE

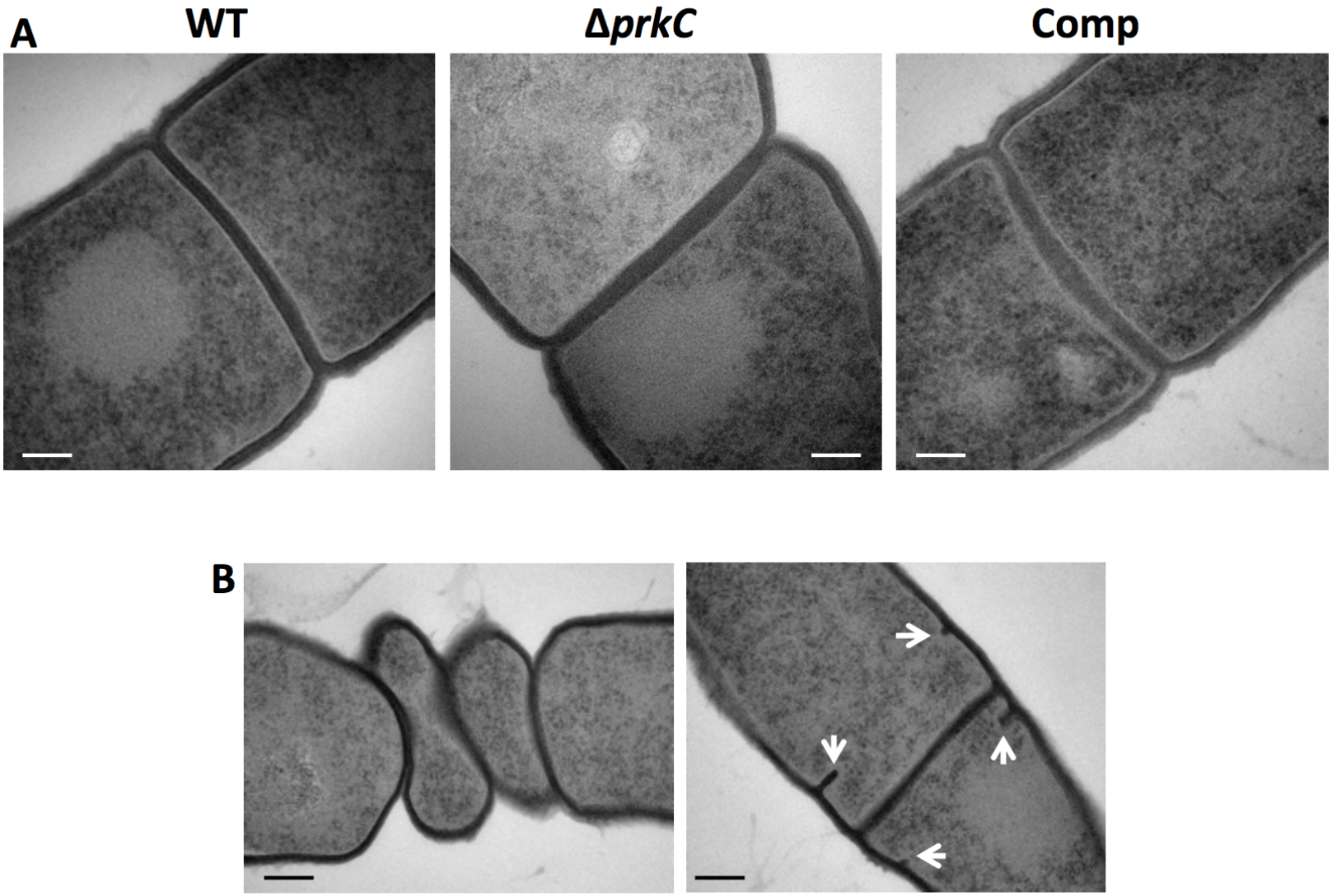
A
WT
ΔprkC
Comp
B

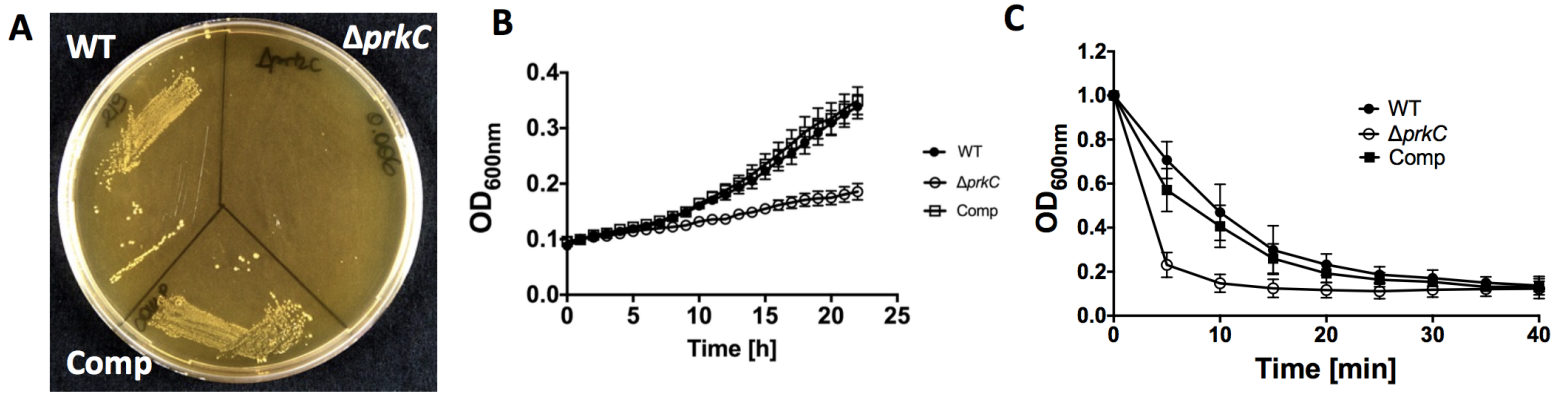
A
WT
ΔprkC
Comp
B
OD600nm
Time [h]
WT
ΔprkC
Comp
C
OD600nm
Time [min]
WT
ΔprkC
Comp

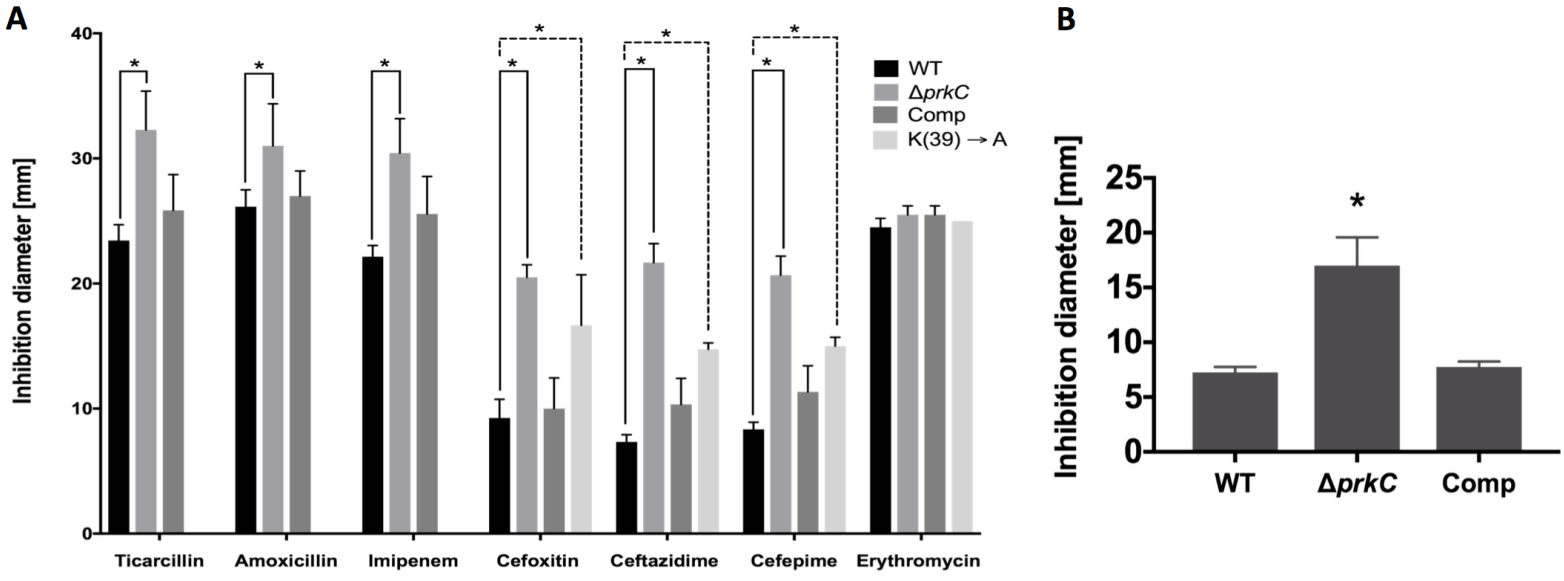
A
Inhibition diameter [mm]
40
30
20
10
0
WT
ΔprkC
Comp
K(39) → A
Ticarcillin
Amoxicillin
Imipenem
Cefoxitin
Ceftazidime
Cefepime
Erythromycin
B
Inhibition diameter [mm]
25
20
15
10
5
0
WT
ΔprkC
Comp

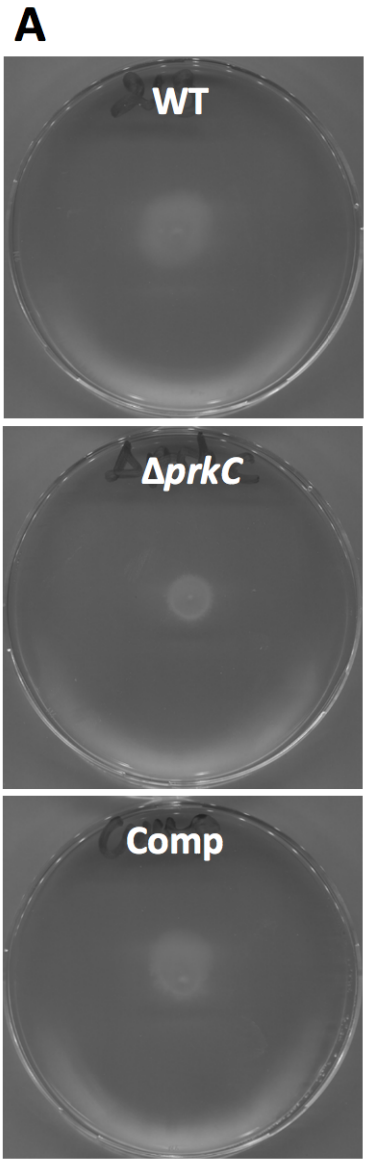
A
WT
ΔprkC
Comp

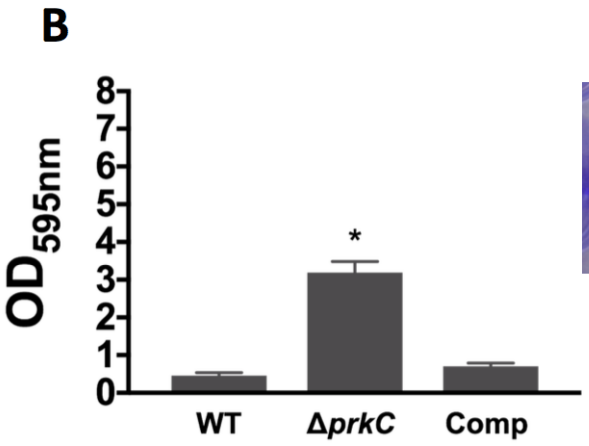
B
OD595nm
0
1
2
3
4
5
6
7
8
*
WT
ΔprkC
Comp

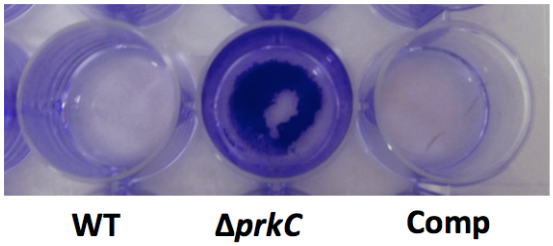
WT
ΔprkC
Comp

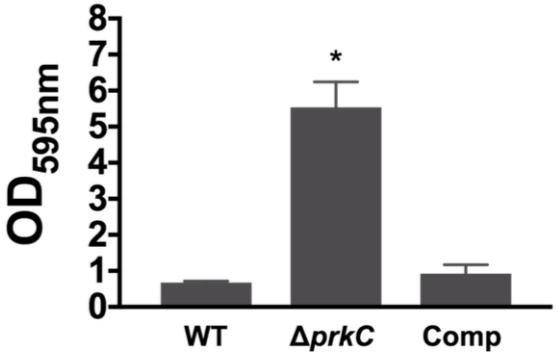
C
OD595nm
0
1
2
3
4
5
6
7
8
*
WT
ΔprkC
Comp

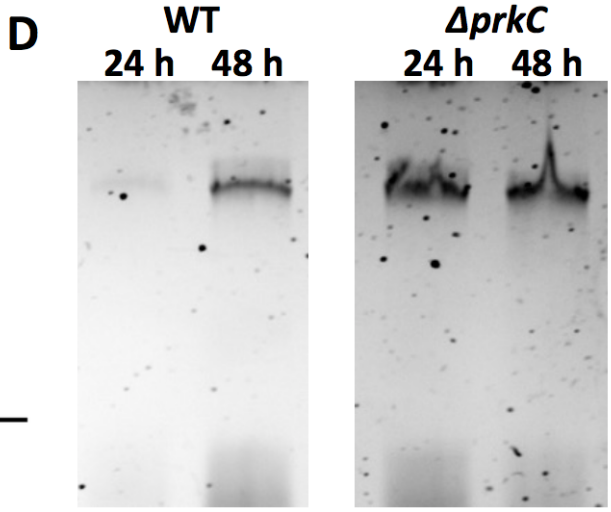
D
WT
24 h
48 h
ΔprkC
24 h
48 h

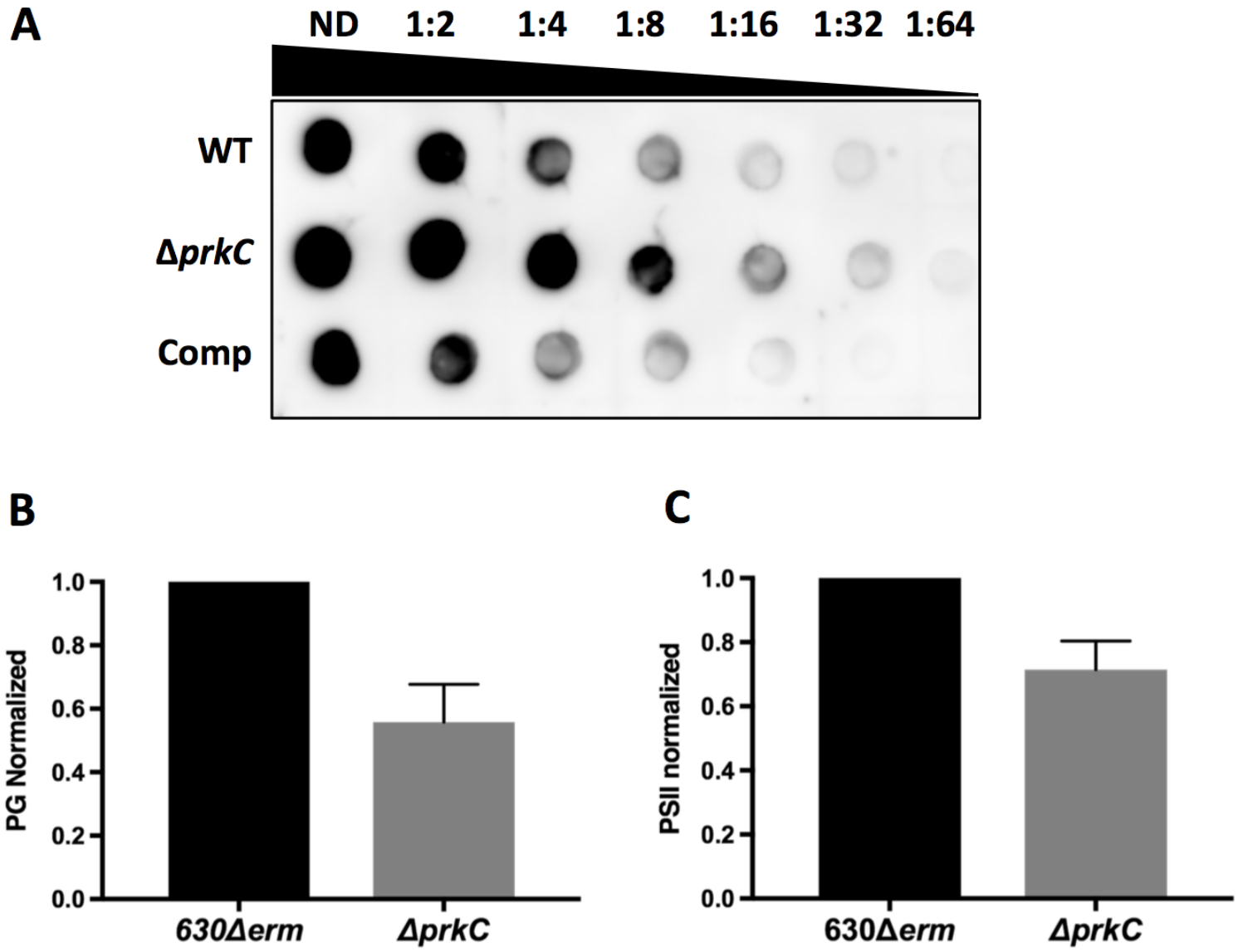
A
ND
1:2
1:4
1:8
1:16
1:32
1:64
WT
ΔprkC
Comp
B
PG Normalized
1.0
0.8
0.6
0.4
0.2
0.0
630Δerm
ΔprkC
C
PSII normalized
1.0
0.8
0.6
0.4
0.2
0.0
630Δerm
ΔprkC

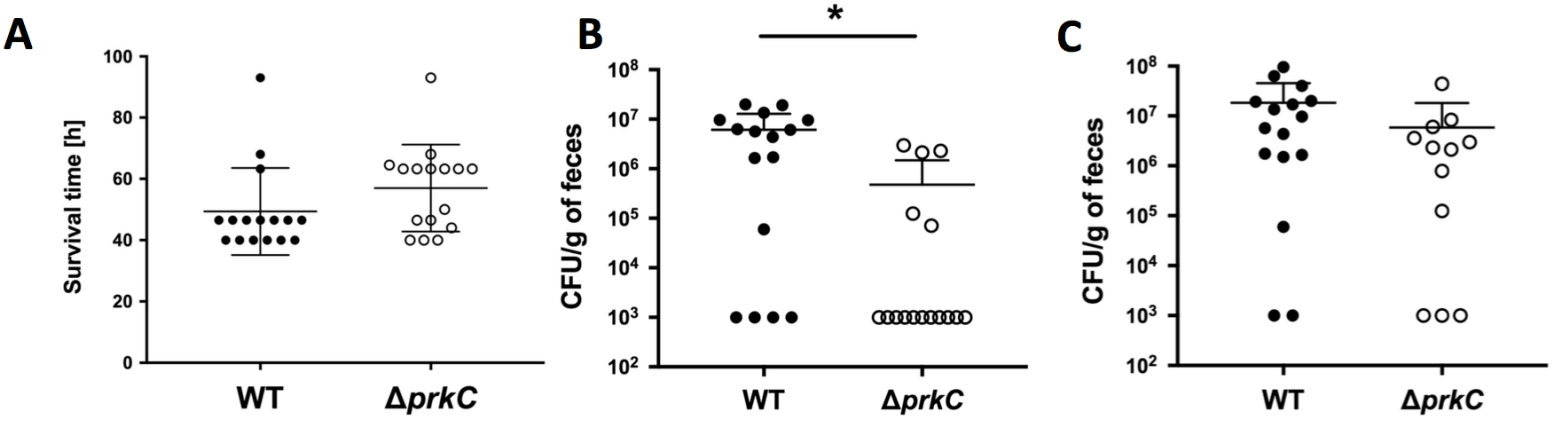
A
Survival time [h]
100
80
60
40
20
0
WT
ΔprkC
B
*
CFU/g of feces
10^8
10^7
10^6
10^5
10^4
10^3
10^2
WT
ΔprkC
C
CFU/g of feces
10^8
10^7
10^6
10^5
10^4
10^3
10^2
WT
ΔprkC